

A Near-Infrared Survey of the Inner Galactic Plane for Wolf-Rayet Stars I. Methods and First Results: 41 New WR Stars

Michael M. Shara

American Museum of Natural History, 79th Street and Central Park West, New York, NY,
10024-5192

mshara@amnh.org

Anthony F. J. Moffat

Département de Physique, Université de Montréal, CP 6128 Succ. C-V, Montréal, QC,
H3C 3J7, Canada

moffat@astro.umontreal.ca

Jill Gerke

American Museum of Natural History, 79th Street and Central Park West, New York, NY,
10024-5192

jgerke@amnh.org

David Zurek

American Museum of Natural History, 79th Street and Central Park West, New York, NY,
10024-5192

dzurek@amnh.org

Kathryn Stanonik

Department of Astronomy, Columbia University, 550 West 120th Street, New York, NY
10027

keejo@astro.columbia.edu

René Doyon

Département de Physique, Université de Montréal, CP 6128, Succ. C-V, Montréal, QC,
H3C 3J7, Canada

doyon@astro.umontreal.ca

Etienne Artigau

Gemini Observatory, AURA, Casilla 603, La Serena, Chile

eartigau@gemini.edu

Laurent Drissen

Département de Physique, Université Laval, Pavillon Vachon, Quebec City, QC, G1K 7P4
Canada

ldrissen@phy.ulaval.ca

Alfredo Villar-Sbaffi

Département de Physique, Université de Montréal, CP 6128, Succ. C-V, Montréal, QC,
H3C 3J7, Canada

alfredovs@hotmail.com

Received _____; accepted _____

Submitted to AJ

ABSTRACT

The discovery of new Wolf-Rayet (WR) stars in our Galaxy via large-scale narrowband optical surveys has been severely limited by dust extinction. Recent improvements in infrared technology have made narrowband-broadband imaging surveys viable again. We report a new J, K and narrow-band imaging survey of 300 square degrees of the plane of the Galaxy, spanning 150 degrees in Galactic longitude and reaching 1 degree above and below the Galactic plane. The survey has a useful limiting magnitude of $K = 15$ over most of the observed Galactic plane, and $K = 14$ within a few degrees of the Galactic center. Thousands of emission line candidates have been detected. In spectrographic follow-ups of 173 WR star candidates we have discovered 41 new WR stars, 15 of type WN and 26 of type WC. Star subtype assignments have been confirmed with K band spectra, and distances approximated using the method of spectroscopic parallax. A few of the new WR stars are amongst the most distant known in our Galaxy. The distribution of these new WR stars is seen to follow that of previously known WR stars along the spiral arms of the Galaxy. Tentative radial velocities were also measured for most of the new WR stars.

Subject headings: Galaxy: disk — Galaxy: stellar content — Galaxy: Population I — stars: emission line — stars: Wolf-Rayet — surveys

1. Introduction

1.1. Motivation

It is extraordinary but true that the galaxy of the Local Group whose global stellar populations are least well observed is our own Milky Way. Deeply immersed within the optically opaque, dusty lanes of our Galaxy’s spiral arms, astronomers have been frustrated for centuries in their attempts to map the stellar populations of the Milky Way. A complete census of our Galaxy for every member of even one class of star would have seemed like an impossible goal even a decade ago. Major advances in instrumentation are transforming this daunting task from near-impossibility to increasingly likely. Wide-field, high-resolution, sensitive surveys, particularly in the near-infrared and X-ray parts of the electromagnetic spectrum (where the Galaxy is relatively transparent), are key to locating and characterizing all members of one or more classes of stellar object. The goal of the project described in this paper is to detect and spectrographically characterize at least 90% of the Wolf-Rayet stars in the Milky Way within ten years.

A set of well-defined tests of stellar evolution theory will follow from detections of complete samples of Wolf-Rayet and other related stars. For example, the radial abundance gradient across our Galaxy and the increase of the WR/O number-ratio with increasing Z suggests that many more WR stars will be found in the inner parts of the Milky Way than in the outer regions. In addition, our previous HST survey of the HII regions in the ScIII galaxy NGC 2403 (Drissen et al 1999) suggested that the distribution of Wolf-Rayet and red supergiant stars (RSG) is a sensitive diagnostic of the recent star-forming history of these large complexes: young cores of O and WR stars are surrounded by older halos containing RSG. Theory predicts that the number-ratio WR/O increases with increasing metallicity; thus, relatively fewer WR stars form at lower Z . We will also be able to determine if superclusters, dominated by Wolf-Rayet stars, are common in the Milky Way.

Finally, we note that WR stars are predicted to end their lives as supernovae, and in rare cases as Gamma Ray Bursts. The Wolf-Rayet stars in the Milky Way may be abundant enough for one to erupt as a Type Ib or Ic supernova within a few generations. This comes from the assumption that the MW contains ~ 6000 WR stars, each lasting $\sim 5 \times 10^5$ yrs. The clear identification of a WR star as the progenitor of one of these eruptions would be a dramatic confirmation of a key prediction of stellar evolution theory.

1.2. Wolf-Rayet stars

Wolf-Rayet (WR) stars are massive (with initial masses greater than $\sim 20M_{\odot}$ at Z_{\odot}) stars with strong winds ($\dot{M} \sim 10^{-5}M_{\odot}yr^{-1}$) displaying the heavier elements created by what are normally internal nuclear processes. Distinctive spectra with strong, broad emission lines of helium, and either nitrogen (WN) or carbon (WC) are the defining observational characteristics of WR stars. As they have relatively short lifetimes (about 5×10^5 years), WR stars are excellent tracers of star formation, and they are also believed to be type Ib or Ic supernova progenitors, because they have removed their outer H-rich layers (WN) or even He-rich layers (WC/O).

About 300 WR stars have been previously identified in the Milky Way (van der Hucht 2006), with distribution models predicting ~ 1000 -6500 total expected (Shara et al. (1999); van der Hucht (2001)). Optical narrow band surveys have been severely limited by interstellar extinction (Shara et al. 1999), and so the natural solution is to turn to the near infrared. Emission line magnitudes of 40 known WR stars are presented in Appendix A. A model of the Milky Way, predicting the numbers and distributions of WR stars visible in the K band is presented in Appendix B.

In an initial attempt at a narrowband near-infrared survey Homeier et al (2003) had

limited success, while Hadfield et al (2007) were somewhat more successful with their color-based selection of objects from the 2MASS (Skrutskie et al 2006) and GLIMPSE (Benjamin et al 2003) surveys.

Utilizing a new narrow-band survey, described in § 2 along with the candidate selection methods, we have found 41 new WR stars: 15 WN and 26 WC. Spectrographic follow up and data reduction is described in § 3. Our resulting K-band spectra, line measurements, and subtype classification are presented in § 4. Distances to the new WR stars are calculated and their distribution within the Galaxy considered in § 5. Our conclusions are summarized in § 6.

2. Observations

The most reliable optical technique to detect individual Wolf-Rayet stars in crowded fields consists of subtracting a normalized continuum image from an image obtained with a narrowband filter centered on the HeII 4686Å line. This works well for individual WR stars with equivalent widths of HeII(4686) 10 – 15 Å or larger, and even for dense, unresolved clusters that include a very small fraction of WR stars (Drissen et al (1993)). Unfortunately, dust extinction makes this technique infeasible for the large majority of Galactic WR stars. Only in the near-infrared can we hope to detect the WR stars farther than about 5 kpc.

A near-infrared survey of the plane of the Galaxy was carried out under the umbrella of the SMARTS consortium (see <http://www.astro.yale.edu/smarts/>). The imaging data were taken over approximately 200 nights in 2005-2006 on the Cerro Tololo Inter-American Observatory (CTIO) 1.5 meter telescope, using the Université de Montréal’s CPAPIR camera. Images are 35’ on a side, with a plate scale of 1.03’’ per pixel, and cover 1° above

and below the Galactic plane from Galactic longitude $l=-90^\circ$ to $l=60^\circ$. Each of the 1200 fields was imaged in the J and K bands, and through a selection of narrow bands designed for identifying WR stars.

Motivated by the WR infrared spectra in Figer et al. (1997), we purchased a filter set (Table 1) which targeted the emission line features He I 2.062 μm , C IV 2.081 μm , H I Br γ 2.169 μm , and He II 2.192 μm . In addition, two narrow-band continuum filters were used which were selected to be relatively devoid of emission lines, one blueward (2.033 μm) and one redward (2.255 μm) of the emission line filters. These were then used to linearly interpolate a continuum magnitude at each of the emission line bands, so we could calculate the difference in measured and interpolated magnitudes, Δm , indicative of emission or absorption in that band. In this paper, we are working from a catalogue of the calculated Δm values for all of the stars contained in the survey area which had been processed by the time of our spectroscopic follow-up. This consisted of about 75% of the survey area, and in general we excluded those areas most crowded with stars, in particular the approximately eight degrees in longitude closest to the Galactic center.

2.1. Image Processing

The more than 77,000 science and dome flat images of the survey require a customized, streamlined pipeline to reduce this large amount of data. The pipeline was constructed (by JG and DZ) in IDL and uses the 2MASS catalogue extensively as a reference for both astrometry and photometry. Each of the ~ 1200 fields has been imaged in each of the 8 filters at 7 dither positions with separations of $\sim 15''$. Dome flats were used to flatten each of the images for sensitivity and chip defects. These 7 dither positions were median combined together without shifting to remove most of the stellar sources and to create a sky image. The sky image was subtracted from each image.

Sources for each field/filter were matched to 2MASS to determine the world coordinate system (WCS). Once a WCS was fit, another iterative process was performed to minimize the residuals to 2MASS and determine the best geometric distortion solution. The IDL procedure `WARP_TRI` applied the geometric distortion solution. The IDL procedure `HASTOM` aligned all the images taken in a dither series. These images were combined to create a final deep exposure.

2.2. Photometry

Sources were identified as WR candidates through emission in the narrowband filters. This made it necessary to have not only the magnitude of a source in the narrowband filter, but also the magnitude of the continuum at that wavelength. As a result, each narrowband filter had to be examined concurrently with the `CONT1` and `CONT2` filters.

Sources on the final deep exposures were detected using the IDL procedure `FIND`. Aperture photometry was then carried out using the IDL procedure `APER` with a 2-pixel aperture and a sky annulus from 10 to 20 pixels. Objects matched to the 2MASS catalog (at least 100 in each field) were used to determine a zero point for each filter in each deep image. An object with a flat spectrum through our filters has the same magnitude in all 6 filters.

Sources were considered matched across filters if their positions were consistent within 0.5 pixel. These matched sources with 2MASS-calibrated magnitudes were then used to construct emission-magnitude diagrams (EMDs). An EMD was constructed for each narrowband filter with the wavelength-interpolated continuum magnitude vs continuum-subtracted narrowband magnitude. The stars scatter around a continuum-subtracted narrowband magnitude of zero. In each magnitude bin we calculate the standard deviation

sigma of the continuum-subtracted narrowband magnitude. Objects that are 5σ or more in the negative direction from the locus of stars are considered candidates. We determined the offset to convert instrumental magnitudes to apparent magnitudes using the 2MASS Ks band catalogue. The images were divided into an 8x8 grid, with each of the 64 areas having an individually determined offset, to compensate for an observed color dependence (probably due to variable reddening) across the field. The IDL procedure APER determined the magnitude for the source at the coordinates given by 2MASS.

Once the offsets to convert to apparent magnitude were calculated, FIND, an IDL procedure, identified sources in an image that were a given deviation above the background. APER found the instrumental magnitude for the sources, which were then converted to apparent magnitudes. The CONT1 filter was taken as a reference image and HASTROM aligned all filters from a field. The sources from CONT1 were then matched to the sources from the CONT2 image and sources within 0.5 pixels were kept as matches. The matched sources were then compared to the sources of a narrowband filter. The result was a list of sources found within 0.5 pixels of each other in both of the continuum filters and the narrowband filter. A linear fit was found between the CONT1 and CONT2 filter magnitudes of each source. Then, using the central wavelength for the narrowband filter, an interpolated continuum value at the narrowband wavelength was determined. The magnitude of the source in the narrowband filter was then subtracted from the interpolated continuum value, giving the negative emission magnitude for the source in that narrowband filter. The emission magnitude for a source was also estimated by subtracting the CONT1 and the CONT2 magnitude from the narrowband magnitude, resulting in a total of three estimates for the emission magnitude of a source. An EMD of continuum magnitude vs. emission magnitude was created for each narrowband filter and the standard deviation was determined for the sources in bins of 1 magnitude. Sources that had emission magnitudes of 5σ or greater from the center of the EMD were marked as WR candidates. $1 \text{ arcmin} \times$

1 arcmin finder charts were produced for each WR candidate, showing the candidate in all filters of the survey and also in XDSS red and XDSS infrared images. These are presented in Appendix C. Candidates with emission magnitudes that were similar to those of the known WR stars covered in the survey were selected for spectrographic follow up. This refined list of candidates was blinked by eye to remove any candidates that did not resemble stars.

2.3. Candidate Selection

In this initial, exploratory phase of the survey we used two techniques when selecting targets for spectroscopic follow-up. We began by selecting targets with such powerful emission lines that the star appeared brighter in the narrow-band images when compared to the continuum images even when examined by eye. This corresponds to a minimum 0.5 to 1 magnitude difference in brightness between the narrow- and broad-band images. We initially selected candidates displaying a brightening of at least 0.5 magnitudes in at least one narrow band image relative to the continuum. This resulted in the detection of 34 new planetary nebulae (which will be reported elsewhere) whose very strong, sharp emission lines, He I 2.058 μm and Br γ 2.166 μm , fell within our He I and Br γ narrow-band imaged fields. A few of the planetary nebulae were slightly resolved on the Br γ narrow-band images. No new WR stars have yet been found this way.

Our second, much more successful, technique relied on using known WR stars to calibrate our selection of targets. Forty known WR stars were selected within the survey area, and patterns were found in their narrow band Δm values which distinguished broad subtypes of WR stars. (See Appendix A). WC stars generally showed strong (-0.8 magnitudes or less) emission excess in the C IV filter, and slightly weaker emission (between -0.4 and -0.8 magnitudes) in the He I filter, due to the blue side of the C IV line extending

into the range of the He I narrow-band filter. Early WN stars generally showed moderate emission in the Br γ filter and the He II filter, but slight absorption (0.1 magnitudes) in both He I and C IV.

Using these criteria, 173 candidate targets were selected which appeared at least 5σ brighter in their narrow-band filter than did other stars in the field and which also fit the criteria suggested by the known WRs. Though we are reliably detecting stars to magnitude 14-14.5 in all of the filters (by judicious choice of exposure times), during this exploratory stage candidates were selected to have emission-band magnitudes brighter than $K = 11.5$. This is because the initial spectrographic follow-up is being done with a 1.5m telescope (see below). (Thousands of uncrowded 5σ candidates as faint as faint as $K = 14.5$ will be the subjects of future papers). There are strong selection effects for those WR subtypes which were used to determine the selection criteria, and as a result, no WC9 or late WN type ($>WN6$) stars have yet been found. Improvements now underway in survey image reduction will permit discovery of the less strongly distinguished subtypes.

3. Spectrographic Observations and Reduction

The spectrographic follow-up data were taken between 28 April and 6 June 2007, with the near-infrared (0.8 - 2.5 μm) SIMON spectrograph (Doyon et al 2000) of the Université de Montréal mounted on the 1.5 meter telescope at CTIO. SIMON has a scale of 0.46 "/pixel on the CTIO 1.5 meter telescope. Targets were observed in the K band with a resolving power of $R \sim 1500$. Each target was observed 5 times, with a nod to move the target along the slit between each observation. Total integration times ranged from 10 to 30 minutes per candidate.

All data were reduced using IRAF routines. Images were dark subtracted and flat

fielded to remove any instrument signature; spectra were then extracted using the APALL task. This task also provided sky subtraction by fitting the background on either side of the object along the slit. The five exposures were scaled and median-combined. Standard stars, which were observed periodically throughout the night, were similarly reduced, and corrections made for Br γ absorption in the telluric standard. Object spectra were then divided by the temporally closest standard-star spectra to remove, as best as possible, the atmospheric absorption features, particularly those at 2.008 μm and 2.059 μm , and a fainter feature at 2.199 μm .

Wavelength calibrations were done using the atmospheric OH emission observed off-target by the spectrograph during each object observation. Lines were first identified using the IDENTIFY task and were compared with the coordinate list ohlines.dat included therein (Steed & Baker (1979)). The wavelength solution was then refitted to each observed target using the REIDENTIFY task. In general, the root-mean-square error of the residuals of wavelength fits was less than 1 \AA , and in most cases between 0.1 and 0.3 \AA . These dispersion solutions were each applied to the corresponding target object, and then corrected for the intrinsic heliocentric motion using the RVCORRECT task to identify the heliocentric velocity and the DOPCORRECT task to Doppler shift the wavelength scale.

4. Results

From our target list of 173 candidates we have discovered 41 new Wolf-Rayet stars: 15 of type WN and 26 of type WC. Right ascension and declination, as well as J, H and K_S magnitudes, were obtained from 2MASS, and are listed in Table 2. All 2MASS objects were then referenced in NOMAD (Zacharias et al 2005) to obtain B, V, and R magnitudes, when available, which are also included in Table 2. Spectra are grouped by assigned spectral type, and are presented in Figures 1a through 1k.

4.1. Spectral Line Measurements

The IRAF task SPLIT was used to fit the continuum and then optimize and deblend Gaussian functions to fit the observed emission lines in all spectra. This gave measurements of line centers, equivalent widths (EWs) and the full-widths-at-half-maximum (FWHMs).

A number of errors contribute to reduce the accuracy of these measurements. Blending of many lines creates the largest emission features, and introduces errors into line center measurements up to 10 Å. It also skews the shape of the feature to be a poor fit to a Gaussian. In general, the rms error of the residuals for the fits was about 10% of the continuum value. Additionally, the continuum was quite difficult to determine precisely due to the abundance of emission lines throughout the spectrum, especially in WC stars, resulting in errors in the equivalent width measurements. A number of our WN detections were rather faint, with peak fluxes only twice the continuum level, resulting in lower signal-to-noise ratios for these spectra. Finally, ground-based observatories must peer through the murky atmosphere, so that the strong C IV 2.08 μm line in WC stars falls on the edge of the equally strong atmospheric absorption feature at 2.06 μm . Division by a standard star removes most of this feature; however, changes in atmospheric conditions between object and standard-star observations result in residual features on the blue side of the emission line.

4.2. Spectral Classification

The strong emission lines visible in the spectra, while easily distinguished as belonging to either type WC or WN, are the result of overlapping blends of emission lines of various elements. In the optical, WR stars are categorized by looking at ratios of equivalent widths of various nitrogen species for WN, carbon and oxygen species for WC, and He II and He I

for both. However, the heavy blending of lines present in the K band makes it more difficult to find either isolated spectral lines or distinguishing ratios of blended lines (Figer et al 1997).

Spectral subtypes were assigned following Crowther et al (2006). These are presented in Tables 3 and 4, along with the ratio of equivalent widths used for categorization. The ratio $W_{2.189}/W_{2.165}$ was used to categorize the WN stars, and the ratio $W_{2.076}/W_{2.110}$ was used to categorize the WC stars. Also following Crowther et al (2006), WN stars with $\text{FWHM}(\text{He II } 2.189) \geq 130\text{\AA}$ were classified as broad/strong, and the letter 'b' appended to the subtype designation. Subtypes thus assigned are expected to be accurate to within one subtype. The 40 known WR stars were similarly assigned subtypes, which agreed within one subtype of their published spectral classifications.

Those WC stars with especially broad, heavily blended C IV and C III lines, as presented in Figure 1e and which match our observed spectra of WR19 (WC4) and spectra observed in Figer et al (1997) of WR146(WC4), WR143(WC5) and WR150(WC5), are classified more generally as WCE.

4.3. Measured Line Centers

Blended lines complicate the calculations of accurate radial velocities, as there is no longer any fixed line-center with which to compare theoretical and actual wavelengths. The purest line in our K band spectra, He II at 21891 Å, allows measurement of radial velocity with respect to the motion of the sun in principal; however, this line is extremely weak or not discernable in most of the WC stars. Line-center measurements are further complicated by the difficulty of accurately fitting Gaussian curves to WR emission lines, as described in section 4.1, resulting in errors of 5-10 Å in determination of peak wavelengths. This

corresponds to errors on the order of 50-150 km/s. In general, the direction of motion with respect to the Sun follows the clockwise rotation of the Galaxy; however, as noted, the error on these measurements is large. Measured radial velocities (based on the measured line centers, which may be shifted, depending on details of the line formation mechanism) for WNs and, when possible, WCs, are included in Tables 3 and 4.

5. WR Distribution

Distances to all new WR stars were estimated from the 2MASS J, H and K_S color excesses, using the method of spectroscopic parallax described in Crowther et al (2006). Intrinsic $J - K_S$ and $H - K_S$ colors specific to WR subtype were taken from Crowther et al (2006) and used to calculate E_{J-K_S} and E_{H-K_S} . Extinction ratios taken from Indebetouw et al. (2005) then allow two calculations for A_{K_S} :

$$A_{K_S} = 0.67^{+0.07}_{-0.06} E_{J-K_S} \quad (1)$$

and

$$A_{K_S} = 1.82^{+0.30}_{-0.23} E_{H-K_S} \quad (2)$$

The average of these values, $\overline{A_{K_S}}$, was used to calculate the distance modulus, taking the apparent K_S magnitude from 2MASS and the subtype-specific absolute magnitude, M_{K_S} , from Crowther et al (2006). Derived K_S band extinctions and Galactocentric distances, R_G , are listed in Table 5. Calculations for R_G assume the IAU standard Solar Galactocentric distance $R_\odot=8.0$ kpc., and the known Galactic WR stars are on the same scale in Figure 2. Because these calculations are based on the inherent absolute magnitude and $J - K_S$ and $H - K_S$ colors for each subtype, the errors are highly dependent on the accuracy of these measurements. The measured scatter about the adopted color values is

approximately 0.02 magnitudes (table A1 in Crowther et al (2006)), which is negligible in A_{K_S} compared to the average scatter of 0.4 magnitudes from the adopted M_{K_S} values. The redundant calculations of A_{K_S} also provide some indication of the reliability of our measurement. The two values are generally in agreement to within 0.2 magnitudes, especially for the WNs, however they can differ by as much as 0.66 magnitudes for some of the WCs, indicating that more accurate subtype specific colors and absolute magnitudes are needed. These uncertainties give typical errors on the order of 25% in our distance measurements, though they may range as high as 40% in some cases.

The distances to new stars were constrained by the limiting observable magnitude of $K_S \sim 11.5$. Using the overall average extinction $A_{K_S} = 1.4$, we can calculate the typical measurable distances by subtype. As all discovered WN stars were early types, we can distinguish the faintest observed, strong and weak-lined WN as having average distances of 8.0 and 9.4 kpc, respectively, while observations of the faintest WC stars yield typical distances of 8.9 kpc.

In Figure 2 our new WR stars (in bold) have been over-plotted with the previously-known WRs onto the plane of the Galaxy, with distances to the known stars taken from the 7th catalogue of Galactic Wolf-Rayet stars (van der Hucht 2001). The Galactic center is labeled, and circles of radius 4, 8, and 12 kpc are plotted. The new WR stars largely follow the distribution pattern established by the known stars, though we can see that we are beginning to push out to larger heliocentric distances. We also find new stars without optical counterparts within a few kpc of our Sun, reinforcing the necessity of WR surveys in the near infrared. Conti & Vacca (1990), along with the more recent reanalysis in Hadfield et al (2007), maintain that WR stars trace the spiral structure of the galaxy. One arm may be seen along roughly the 8 kpc radius, and an inner arm can perhaps begin to be traced along the inner 4kpc radius. However, the distance error bars are not trivial, so that

firm conclusions about the utility of WR stars as spiral tracers should not yet be drawn.

6. Conclusions

We have discovered 41 new Galactic WR stars, 15 of type WN and 26 of type WC, using a new, near-infrared narrow-band survey of the Galactic plane. The reduced extinction from dust and gas in the near infrared makes this the optimal method for future discovery of the thousands of undetected Galactic WR stars. Of the 254 total candidates observed spectrographically, 75 proved to be emission line objects. All of the emission line objects that were not WR stars (34 objects) were planetary nebulae (PN). As the key goal of this survey is the detection of new Galactic WR stars, we amended our selection criteria to eliminate likely PN. Our modified selection criteria yielded 173 WR star candidates which were observed spectrographically: 41 proved to be new WR stars. With such a 23% detection rate, we have barely scratched the surface of the wealth of new WR stars expected to be discovered within our survey area with the available data.

An initially fairly simple sky-subtraction methodology resulted in relatively scattered color-magnitude diagrams, raising our cut for emission objects to 5σ . It also meant that most of our non-detections were erroneously selected objects with featureless spectra. Improved sky subtraction (using entire nights of data, median-filtered in each filter as skyflats) will allow us to lower this limit to 3σ and will improve the detection rate of emission-line objects. We expect this survey to yield thousands of additional discoveries in the coming years.

Our survey limits will be pushed fainter by the use of a larger infrared telescope for spectroscopic follow-up. As we increase the number of known stars, we will also increase the statistical significance of distribution plots, and subtype abundances, allowing us to

learn more about our Galaxy's structure and composition. The Galactic center is expected to prove an especially rich area for discovery, but it is still largely terra incognita as the crowding of stars there is very high. The vast majority of Galactic Wolf-Rayet stars remain to be discovered, but we now have a proven technique to continue the search.

REFERENCES

- Benjamin, R.A., Churchwell, E., Babler, B.L., Bania, T. M., Clemens, D. P., Cohen, M., Dickey, J. M., Indebetouw, R., Jackson, J. M., Kobulnicky, H. A., Lazarian, A., Marston, A. P., Mathis, J. S., Meade, M. R., Seager, S., Stolovy, S. R., Watson, C., Whitney, B. A., Wolff, M. J., & Wolfire, M. G. 2003, *PASP*, 115, 953
- Buckalew, B.A., Kobulnicky, H.A., Dufour, R.J. 2005, *ApJS*, 157, 30
- Clark, J.S. & Negueruela, I. 2002, *A&A*, 396, 125
- Crowther, P.A., Hadfield, L.J., Clark, J.S., Negueruela, I. & Vacca, W.D. 2006, *MNRAS*, 372, 1407
- Conti, P. S., & Vacca, W. D. 1990, *AJ*, 100, 431
- Doyon, R., Nadeau, D. & Vallee, Ph. 2000, *ASP Conf. Ser.* 195, 548
- Drissen, L., Moffat, A.F.J. & Shara, M. M. 1993, *AJ*, 105, 1400
- Drissen, L., Roy, J-R, Moffat, A.F.J. & Shara, M. M. 1999, *AJ*, 117, 1249
- Drimmel, R., & Spergel, D. N. 2001, *ApJ*, 556, 181
- Figer, D.F., McLean, I.S. & Najarro, F. 1997, *ApJ*, 486, 420
- Hadfield, L.J., Crowther, P.A., Schild, H. & Schmutz, W. 2005, *A&A*, 439, 265
- Hadfield, L.J., van Dyk, S.D., Morris, P.W., Smith, J.D., Marston, A.P., Peterson, D.E. 2007, *MNRAS*, 376, 248
- Homeier, N.L., Blum, R.D., Pasquali, A., Conti, P.S. & Daminieli, A. 2003, *A&A*, 408, 153
- Indebetouw, R., et al. 2005, *ApJ*, 619, 931

- Massey, P., Conti, P.S., Moffat, A.F.J. & Shara, M.M. 1987, PASP, 99, 816
- Meynet, G., & Maeder, A. 2005, A&A, 429, 581
- Moffat, A.F.J., Drissen, L. Shara, M.M. 1994, ApJ, 436, 183
- Moffat, A.F.J. & Shara, M.M. 1987, ApJ, 320, 266
- Shara, M.M., Moffat, A.F.J., Smith, L.F., Niemela, V.S., Potter, M. & Lamontagne, R. 1999, AJ, 118, 390
- Shorlin, S.L., Turner, D.G., & Pedreros, M.H. 2004, PASP, 116, 170
- Skrutskie, M. F., Cutri, R. M., Stiening, R., Weinberg, M. D., Schneider, S., Carpenter, J. M., Beichman, C., Capps, R., Chester, T., Elias, J., Huchra, J., Liebert, J., Lonsdale, C., Monet, D. G., Price, S., Seitzer, P., Jarrett, T., Kirkpatrick, J. D., Gizis, J. E., Howard, E., Evans, T., Fowler, J., Fullmer, L., Hurt, R., Light, R., Kopan, E. L., Marsh, K. A., McCallon, H. L., Tam, R., Van Dyk, S., & Wheelock, S. 2006, AJ, 131, 1163
- Smartt, S.J., & Rolleston, W.R.J. 1997, ApJ, 481, 47
- Steed, A.J. & Baker, D.J. 1979, Appl. Opt., 18, 3386
- Tutukov, A.V., & Cherepashchuk, A.M. 2003, Astronomy Reports, 47, 386
- Vanbeveren, D., Van Bever, J. & Belkus, H. 2007, ApJ, 662, 107
- van der Hucht, K.A. 2001, New Astronomy Review, 45, 135
- van der Hucht, K.A. 2006, A&A, 458, 453
- Zacharias, N., Monet, D.G., Levine, S.E., Urban, S.E., Gaume, R., & Wycoff, G.L. 2005, VizieR Catalog I/297

MMS, JG and DZ acknowledge with gratitude Hilary Lipsitz, whose ongoing support has been essential to the success of this program. AFJM, RD, LD are grateful to NSERC (Canada) and FQRNT (Quebec) for financial aid. We also thank the American Museum of Natural History for essential funding, and a careful referee for excellent suggestions. Most of the infrared imaging was expertly carried out by Claudio Aguilera, Alberto Miranda and Alberto Pasten.

APPENDIX A

A. Summary of known WRs contained in Survey Images

In Tables 6 and 7 we give a summary of the emission line Δm values measured for the known WRs found in the survey area. All survey stars were compared with finder charts for the known WR stars to ensure that photometric measurements were made for the correct star. All stars were found by eye to be present in the survey images, though some had not been identified photometrically due to nebulosity and occasional out-of-focus images.

The Δm magnitude for each narrow-band filter gives the difference in magnitude from the interpolated continuum magnitude. Negative values of Δm indicate emission, positive values indicate absorption for lines in the narrow-band emission-line filter, assuming there are no other problems. Several fields were imaged multiple times, and on more than one night. This allowed us to estimate the accuracy of the emission line magnitudes in Tables 6 and 7 as ± 0.03 magnitudes.

APPENDIX B

This manuscript was prepared with the AAS L^AT_EX macros v5.2.

A. The Total Number and Distribution of Galactic WR Stars

Following Shara et al. (1999), we assume that the star distribution expressed in cylindrical galactic coordinates (i.e. $N(r, l, z)$) follows that of the interstellar dust and adopt an axisymmetric exponential disk formulation with an outwards flair taken from Drimmel & Spergel (2001):

$$N(r, l, z) = N_o e^{\frac{-(R(r, l) - R_o)}{\alpha_{RD}}} \sec h^2 \left(\frac{z - z_o}{\alpha_{HD}(R)} \right)$$

With,

$$R(r, l) = \sqrt{r^2 + R_o^2 - 2rR_o \cos l}$$

A linear flair is added by imposing the following functional form to α_{HD} :

$$\alpha_{HD}(R) = \begin{cases} h_o + (R(r, l) - r_f)h_1 & R(r, l) > r_f \\ h_o & R(r, l) \leq r_f \end{cases}$$

In these equations, N_o is the local stellar density, $R_o = 8000$ pc and $z_o = -17$ pc are respectively the solar galactocentric distance and distance from the galactic plane. The scale length α_{RD} and the constants h_o , h_1 and r_f which define the scale height α_{HD} are taken from the fit to the FIR emission of the interstellar dust of Drimmel & Spergel (2001) and are respectively 2260 pc, 134 pc, 0.015 and 4400 pc.

Although the assumption that the star distribution follows the dust is justified for O stars, it must be modified for WR stars to account for the observed metallicity dependence of their galactic distribution. Using the results of Maeder & Meynet (1994) for the metallicity dependence of the WR/O number ratio and the radial metallicity distribution of

the galactic disk from Smartt & Rolleston (1997), Shara et al. (1999) found that the WR star density can be expressed as:

$$N_{WR}(r, l, z) = N_{WR_o} e^{\frac{-(R(r,l)-R_o)}{\alpha_{RWR}}} \sec h^2 \left(\frac{z-z_o}{\alpha_{HD}(R)} \right)$$

Where,

$$\alpha_{RWR} = \frac{1}{\frac{1}{\alpha_{RD}} + 7 \times 10^{-5} \ln 10} = 1657 pc,$$

Knowing the local surface density of WR stars from van der Hucht (2001):

$$\int_{-\infty}^{\infty} N_{WR}(0, 0, z) dz = 2.87 \times 10^{-6} pc^{-2}$$

And applying this constraint to $N_{WR}(r, l, z)$ we obtain:

$$N_{WR_o} = \frac{2.87 \times 10^{-6} pc^{-2}}{\int_{-\infty}^{\infty} \sec h^2 \left(\frac{z-z_o}{\alpha_{HD}(0)} \right) dz} = 2.09 \times 10^{-8} pc^{-3}$$

Finally, the conversion of the WR star density from a spatial ($N_{WR}(r, l, z)$) to a magnitude ($\eta_{WR}(m, l, z)$) dependence is done in two steps. First, we use the conservation of stars in both systems to write:

$$\eta_{WR} dm dl dz = N_{WR} r dr dl dz$$

Then, the radial distance r is converted to the magnitude k using the inverse square-law of light attenuation accounting for interstellar extinction:

$$5 \log r - 5 = k - M_k - \int_0^r a_k(r, l, z)$$

where the extinction $a_k(r, l, z)$ allowing for a spherical hole in the interstellar dust at the center of the Galaxy is (see Drimmel & Spergel 20001):

$$a_k(r, l, z) = \begin{cases} a_{k_o} e^{\frac{-(R(r,l)-R_o)}{\alpha_{RD}}} \operatorname{sech}^2\left(\frac{z-z_o}{\alpha_{HD}(R)}\right) & R(r, l) \geq 0.5R_o \\ a_k(0.5R_o, l, z) e^{-\left(\frac{R(r,l)-0.5R_o}{2500}\right)^2} & R(r, l) < 0.5R_o \end{cases}$$

with $a_{k_o} = 1.08 \times 10^{-4}$ mag/pc (Mathis 1990) and the intrinsic magnitude of WR stars in the K -band $M_k = -4$ mag (van der Hucht 2001).

These equations have been solved numerically to determine the star density $\eta_{WR}(k, l, z)$ to an accuracy better than 1% using a Monte-Carlo method with a Sobol quasi-random number generator in $3D$. By integrating over the whole Galaxy the model predicts ~ 6400 WR stars which is very close to the 6500 predicted by van de Hucht (2001).

Further validation can be carried out by applying this model to the V -band where most WR stars have been detected so far. It is then possible to compare the observed to the predicted number of WR stars. To do so, we adopt $M_V = -5$ mag (van der Hucht 2001) and $a_{V_o} = 1.0 \times 10^{-3}$ mag/pc. According to the model, the number of WR stars observable up to a magnitude of $V = 15, 12$ and 10 are respectively 153, 79 and 42. These numbers are very close to the respective observed numbers reported by van der Hucht (2001) of 159, 80 and 36. It is again apparent how important it is to continue the search for new WR stars in the infrared.

Figure 3 shows the contour plot representing the necessary target K magnitude to detect 95% of all WR stars along a line of sight. Figure 4 shows the number of WR stars expected per CPAPIR field and Figure 5 presents the same information for $K \leq 15$. Figure 6 shows the cumulative number of expected Galactic WR stars as a function of K magnitude. At $K= 11, 12, 13$ and 14 , the expected numbers of Galactic WR stars are 1200, 2500, 4200 and 5400.

APPENDIX C

A. Finder Charts

We present in Figures 7a through 7g the finder charts for the 41 new Wolf-Rayet stars discovered in our survey.

Table 1. The filter central wavelengths, FWHM and exposure times

Filter Name	λ μm	$\Delta\lambda$ μm	Exp-time seconds
CONT1	2.033	0.020	29.70
HeI	2.062	0.010	59.40
CIV	2.081	0.020	29.70
Br- γ	2.169	0.020	29.70
HeII	2.192	0.020	29.70
CONT2	2.255	0.100	10.80

Table 2. New spectrographically confirmed WR stars. Positions and J, H, K_S magnitudes were obtained from 2MASS. B, V, R magnitudes were obtained from NOMAD using their match to 2MASS.

Name	α (J2000)	δ (J2000)	l	b	B	V	R	J	H	K _S
668_4	10 16 26.22	-57 28 05.7	283.26	-0.64	-	-	17.46	11.73	10.38	9.53
740_21	11 16 03.53	-61 26 58.3	291.79	-0.66	16.76	16.82	15.97	13.16	11.57	10.47
740_16	11 19 42.96	-61 27 12.4	292.20	-0.51	13.67	12.35	13.03	11.50	10.99	10.33
768_6	11 46 06.66	-62 47 12.7	295.54	-0.86	15.56	17.17	14.11	12.15	11.36	10.78
772_17	11 50 04.24	-62 52 15.4	296.00	-0.83	18.23	-	16.47	12.57	11.58	10.94
776_3	11 55 52.11	-62 45 02.2	296.62	-0.56	18.38	-	14.94	11.65	10.76	10.14
791_12c	12 13 28.29	-62 41 42.9	298.59	-0.14	-	-	-	14.05	12.67	11.53
808_14	12 28 41.91	-63 25 46.1	300.39	-0.67	20.28	-	17.82	12.78	11.83	10.94
808_23	12 28 50.99	-63 17 00.2	300.40	-0.52	-	-	18.61	13.56	12.55	11.84
807_16	12 30 03.86	-62 50 17.1	300.50	-0.07	-	-	19.20	13.16	12.05	11.09
816_10	12 38 18.78	-63 24 19.7	301.46	-0.57	-	-	18.43	12.93	11.76	10.96
832_25	12 55 44.26	-63 35 50.0	303.41	-0.73	-	-	-	12.48	11.12	10.22
856_13c	13 03 11.08	-63 42 16.2	304.23	-0.86	-	-	18.72	13.13	11.92	11.05
839_12	13 04 50.08	-63 04 40.2	304.45	-0.25	-	-	-	15.69	14.00	12.54
845_34	13 12 21.30	-62 40 12.5	305.33	0.10	-	-	16.24	10.75	9.57	8.77
845_35	13 12 27.67	-62 44 22.0	305.34	0.03	-	-	17.95	13.16	11.82	10.71
847_8	13 12 45.35	-63 05 52.0	305.34	-0.33	-	-	-	13.06	11.34	10.26
853_9	13 22 16.08	-62 30 57.4	306.48	0.14	-	-	-	14.77	12.69	11.55
858_26	13 28 15.87	-62 06 23.5	307.22	0.46	-	-	18.70	12.53	11.40	10.68
883_18	13 52 02.36	-62 26 46.0	309.88	-0.39	-	-	-	14.59	12.41	10.99
885_11	13 54 13.45	-61 50 01.8	310.27	0.14	-	-	-	13.60	12.07	10.86
897_5	14 10 10.01	-61 15 25.5	312.25	0.18	-	-	-	15.30	12.43	10.60
903_15c	14 12 36.54	-61 45 32.7	312.38	-0.38	-	-	-	13.58	11.33	9.71
907_18	14 16 27.37	-61 17 56.2	312.96	-0.09	-	-	-	13.60	11.39	10.01
956_25	15 01 30.11	-59 16 12.0	318.88	-0.49	-	-	-	13.84	11.83	10.64
979_11	15 20 35.91	-57 27 11.9	321.95	-0.20	-	-	-	13.88	12.15	11.06
1011_24	15 43 04.68	-55 11 12.3	325.81	-0.13	19.93	17.31	16.06	10.96	9.94	9.06
1053_27	16 11 43.70	-51 10 16.6	331.67	0.17	-	-	18.53	10.26	8.97	8.10
1059_34	16 14 37.23	-51 26 26.3	331.81	-0.34	-	-	-	15.05	12.79	11.54
1081_21	16 24 58.86	-48 56 52.4	334.75	0.27	-	-	-	13.28	11.76	10.73
1093_34	16 31 29.23	-47 56 16.4	336.22	0.19	-	-	-	15.56	12.86	11.32
1093_33	16 31 49.06	-47 56 04.4	336.26	0.15	-	-	-	15.11	12.86	11.47
1093_53	16 32 12.98	-47 50 35.8	336.37	0.17	-	-	-	15.00	12.70	11.34
1096_22	16 35 23.31	-48 09 18.0	336.51	-0.43	-	-	-	14.90	12.77	11.43
1222_15	17 22 40.74	-35 04 52.9	352.20	0.74	-	-	-	15.11	12.05	10.33
1385_24	18 13 42.47	-17 28 12.2	13.15	0.13	-	-	20.02	11.21	9.70	8.57
1425_47	18 23 03.42	-13 10 00.4	18.01	0.18	15.23	14.49	14.41	10.34	9.28	8.27
1462_54	18 29 33.84	-08 39 02.1	22.75	0.87	-	-	-	14.07	12.75	11.93
1509_29	18 41 48.45	-04 00 12.9	28.27	0.31	-	-	-	15.62	13.32	11.99
1613_21	19 06 36.53	+07 29 52.4	41.33	0.07	-	-	-	14.24	12.65	11.61
1671_5	19 20 40.38	+13 50 35.2	48.55	-0.05	-	-	-	13.57	11.80	10.76

Table 3. Equivalent width (\AA) and FWHM (\AA) measurements for the most prominent lines of the new WN stars. Radial velocities (RV) are measured with respect to the He II line at 21891 \AA , as it is the least blended. Uncertainties of the Ews and FWHMs are typically 20%, while those for the RVs are discussed in the text.

Name	N v		He I		He II + Br γ		He II		$W_{2.189}/$ $W_{2.165}$	RV (in km/s)	Subtype
	(2.100 μm)		(2.115 μm)		(2.165 μm)		(2.189 μm)				
	W_λ	FWHM	W_λ	FWHM	W_λ	FWHM	W_λ	FWHM			
668_4	-8	141	-11	121	-31	147	-91	153	2.9	55	WN5b
740_21	-14	208	-20	200	-39	165	-203	242	5.2	-82	WN4b
768_6	-6	38	-19	126	-42	120	-101	106	2.4	41	WN5
772_17	-3	38	-12	113	-53	126	-95	121	1.8	-	WN6
776_3	-	-	-19	109	-60	93	-72	94	1.2	-	WN6
808_23	-	-	-	-	-46	101	-141	126	3.1	68	WN5
816_10	-	-	-29	227	-48	140	-137	136	2.9	-14	WN5b
847_8	-8	70	-47	142	-65	119	-114	120	1.8	-96	WN6
853_9	-	-	-29	95	-36	66	-92	97	2.6	27	WN6
858_26	-	-	-26	96	-38	74	-56	78	1.5	55	WN6
907_18	-16	171	-19	140	-70	175	-150	153	2.1	-68	WN5b
956_25	-11	202	-35	222	-31	163	-180	366	5.8	-315	WN4b
979_11	-	-	-57	260	-62	207	-212	220	3.4	-14	WN4b
1093_53	-	-	-52	219	-60	185	-145	182	2.4	-68	WN5b
1462_54	-	-	-59	202	-72	164	-166	126	2.3	68	WN5

Table 4. Equivalent width (\AA) and FWHM (\AA) measurements for the most prominent lines of new WC stars. The strong C IV line is a blend of several emission lines. Radial velocities (RV) are measured in km/s with respect to the He II line at 21891 \AA , as it is the least blended, though it is not present in all WC spectra. Uncertainties of the EWs and FWHMs are typically 20%, while those for the RVs are discussed in the text.

Name	C IV		He I + C III		He I		He II		$W_{2.076}/W_{2.110}$	RV	Subtype
	(2.076 μm)		(2.110 μm)		(2.165 μm)		(2.189 μm)				
	W_λ	FWHM	W_λ	FWHM	W_λ	FWHM	W_λ	FWHM			
740_16	-987	255	-226	330	-	-	-50	241	4.4	-	WCE
791_12c	-1590	282	-498	443	-	-	-75	228	3.2	-	WCE
808_14	-948	306	-392	477	-	-	-140	623	2.4	-	WCE
807_16	-985	178	-206	147	-31	103	-74	116	4.8	-55	WC7
832_25	-454	236	-73	236	-37	351	-15	121	6.2	-	WC5-6
839_12	-1658	230	-244	195	-	-	-71	157	6.8	-	WC5-6
845_34	-374	271	-131	284	-	-	-35	384	2.9	-	WC8
845_35	-1789	249	-412	258	-42	323	-70	195	4.3	0	WC7
856_13c	-712	191	-138	180	-14	86	-61	157	5.2	-164	WC5-6
883_18	-1093	301	-373	453	-10	103	-77	320	2.9	-	WCE
885_11	-1489	210	-279	180	-	-	-60	174	5.3	-	WC5-6
897_5	-525	205	-188	165	-56	354	-35	126	2.8	-	WC8
903_15c	-165	186	-66	123	-13	125	-14	125	2.5	-	WC8
1011_24	-884	244	-275	226	-	-	-83	360	3.2	-	WC8
1053_27	-303	222	-81	213	-59	223	-84	202	3.7	-	WC8
1059_34	-729	210	-242	181	-28	366	-44	199	3.0	-	WC8
1081_21	-419	219	-214	174	-75	185	-60	143	2.0	-137	WC8
1093_33	-369	199	-155	161	-69	161	-69	132	2.4	-219	WC8
1093_34	-475	226	-178	222	-62	212	-84	187	2.7	-260	WC8
1096_22	-571	202	-230	156	-71	169	-76	141	2.5	-82	WC8
1222_15	-551	197	-171	154	-	-	-45	230	3.2	-	WC8
1385_24	-537	220	-245	196	-63	361	-33	138	2.2	-	WC8
1425_47	-1593	238	-300	296	-48	250	-75	179	5.3	-	WC5-6
1509_29	-1578	240	-355	224	-	-	-110	273	4.4	-	WC7
1613_21	-659	365	-245	518	-	-	-	-	2.7	-	WCE
1671_5	-335	215	-94	210	-49	337	-20	151	3.6	-	WC8

Table 5. K_S band extinctions and Galactocentric distances for new WR stars. Extinction, K_S , and distance modulus, DM, are given in magnitudes. Uncertainties in the distances are typically 25%.

Distance, d, and Galactocentric radius, R_G , are given in kpc.

Name	Subtype	$A_{K_S}^{J-K_S}$	$A_{K_S}^{H-K_S}$	$\overline{A_{K_S}}$	K_S	M_{K_S}	DM	d	R_G
668_4	WN5b	1.23	1.06	1.14	9.53	-4.77	13.16	4.28	8.60
740_21	WN4b	1.55	1.51	1.53	10.47	-4.77	13.71	5.51	8.24
740_16	WCE	0.37	0.15	0.26	10.33	-4.59	14.66	8.56	9.52
768_6	WN5	0.80	0.76	0.78	10.78	-4.41	14.41	7.62	8.63
772_17	WN6	0.97	0.87	0.92	10.94	-4.41	14.43	7.68	8.60
776_3	WN6	0.89	0.84	0.86	10.14	-4.41	13.69	5.46	7.78
791_12c	WCE	1.27	1.02	1.15	11.53	-4.59	14.97	9.88	9.46
808_14	WCE	0.82	0.56	0.69	10.94	-4.59	14.84	9.29	8.87
808_23	WN5	1.03	1.00	1.02	11.84	-4.41	15.23	11.14	10.02
807_16	WC7	0.97	0.69	0.83	11.09	-4.59	14.85	9.33	8.88
816_10	WN5b	1.07	0.96	1.02	10.96	-4.77	14.71	8.76	8.44
832_25	WC5-6	1.10	0.58	0.84	10.22	-4.59	13.97	6.22	7.26
856_13c	WC5-6	0.98	0.53	0.75	11.05	-4.59	14.89	9.49	8.46
839_12	WC5-6	1.70	1.60	1.65	12.54	-4.59	15.48	12.48	10.39
845_34	WC8	1.04	0.76	0.90	8.77	-4.65	12.52	3.19	7.15
845_35	WC7	1.23	0.96	1.10	10.71	-4.59	14.20	6.93	7.22
847_8	WN6	1.76	1.67	1.71	10.26	-4.41	12.96	3.90	7.01
853_9	WN6	2.04	1.78	1.91	11.55	-4.41	14.05	6.46	6.98
858_26	WN6	1.12	1.02	1.07	10.68	-4.41	14.02	6.37	6.88
883_18	WCE	2.00	1.53	1.76	10.99	-4.59	13.82	5.80	6.53
885_11	WC5-6	1.42	1.15	1.28	10.86	-4.59	14.17	6.81	6.62
897_5	WC8	2.86	2.64	2.75	10.60	-4.65	12.50	3.16	6.79
903_15c	WC8	2.30	2.26	2.28	9.71	-4.65	12.08	2.61	7.01
907_18	WN5b	2.16	2.02	2.09	10.01	-4.77	12.69	3.45	6.65
956_25	WN4b	1.90	1.67	1.79	10.64	-4.77	13.62	5.31	5.70
979_11	WN4b	1.64	1.49	1.57	11.06	-4.77	14.26	7.12	5.26
1011_24	WC8	0.98	0.91	0.95	9.06	-4.65	12.76	3.57	5.90
1053_27	WC8	1.16	0.89	1.03	8.10	-4.65	11.72	2.21	6.64
1059_34	WC8	2.06	1.58	1.82	11.54	-4.65	14.37	7.47	4.01
1081_21	WC8	1.42	1.18	1.30	10.73	-4.65	14.08	6.54	3.80
1093_34	WC8	2.55	2.11	2.33	11.32	-4.65	13.64	5.34	4.21
1093_33	WC8	2.15	1.84	1.99	11.47	-4.65	14.13	6.69	3.59
1093_53	WN5b	2.20	1.98	2.09	11.34	-4.77	14.02	6.36	3.70
1096_22	WC8	2.04	1.75	1.89	11.43	-4.65	14.19	6.88	3.51
1222_15	WC8	2.91	2.44	2.68	10.33	-4.65	12.30	2.89	5.65
1385_24	WC8	1.48	1.37	1.42	8.57	-4.65	11.80	2.29	6.29
1425_47	WC5-6	0.97	0.78	0.88	8.27	-4.59	11.98	2.49	6.18
1462_54	WN5	1.31	1.20	1.26	11.93	-4.41	15.08	10.39	4.16
1509_29	WC7	2.02	1.36	1.69	11.99	-4.59	14.89	9.50	4.50
1613_21	WCE	1.35	0.84	1.09	11.61	-4.59	15.11	10.51	6.97
1671_5	WC8	1.59	1.20	1.40	10.76	-4.65	14.01	6.34	6.41

Table 6. Known WN stars contained in survey, organized by subtype.

WR #	Subtype	Δm_{HeI}	Δm_{CIV}	$\Delta m_{Br\gamma}$	Δm_{HeII}
48c	WN3h+WC4	0.01	0.02	-0.37	-0.20
18	WN4	-0.07	0.06	-0.13	-0.32
35b	WN4	0.10	0.12	-0.18	-0.48
44a	WN4	0.19	-0.22	-0.42	-0.19
45b	WN4	0.11	-	-0.19	0.11
62a	WN4	-0.03	0.01	-0.08	-0.13
31	WN4+O8V	-0.01	0.03	-0.12	-0.21
51	WN4+OB?	-0.08	-0.01	-0.15	-0.38
38a	WN5	0.04	0.02	-0.19	-0.25
42c	WN5	0.09	0.12	-0.16	-0.35
42d	WN5	0.03	0.06	-0.09	-0.29
45a	WN5	0.08	0.05	-0.17	-0.41
36	WN5-6+OB?	0.00	0.08	-0.25	-0.44
111c	WN6	0.08	0.12	-0.21	-0.38
35a	WN6h	0.00	0.01	-0.15	-0.13
21a	WN6+O/a	0.09	-	-0.05	0.02
28	WN6(h)+OB?	0.06	0.06	-0.21	-0.22
47	WN6+O5V	-0.10	0.01	-0.18	-0.19
55	WN7	-0.08	0.03	-0.23	-0.17
74	WN7	-0.06	0.00	-0.17	-0.16
84	WN7	-0.07	0.03	-0.16	-0.22
111d	WN7?	0.03	0.09	-0.04	-0.09
19a	WN7:(h)	-0.06	0.00	-0.20	-0.10
26	WN7/WCE	0.03	-0.59	-0.16	-0.50
107	WN8	-0.23	-0.07	-0.22	-0.02
47b	WN9h	0.08	0.03	-0.26	-0.06
108	WN9h+OB	-0.11	-0.02	-0.01	0.12

Table 7. Known WC stars in survey, organized by subtype.

WR #	Subtype	Δm_{HeI}	Δm_{CIV}	$\Delta m_{Br\gamma}$	Δm_{HeII}
38	WC4	-1.06	-1.56	-	-0.20
47c	WC5	-0.16	-0.42	-0.05	-0.08
32	WC5+OB?	-0.41	-1.77	-0.13	-0.37
41	WC5+OB?	-1.06	-2.52	-0.40	-79.86
23	WC6	-0.46	-	-0.12	-0.28
27	WC6+a	-0.71	-1.36	-0.13	-0.31
31c	WC6+OB	-1.04	-1.51	-0.19	-0.28
38b	WC7+OB	-0.77	-1.14	-0.08	-0.11
39	WC7+OB?	-0.31	-0.76	-0.13	-0.17
42	WC7+O7V	-0.36	-	-0.11	-0.12
50	WC7+OB	-0.76	-1.42	-0.02	-0.15
111b	WC9d	0.12	0.18	-0.11	-0.19
48b	WC9d	-0.03	-0.06	-	-0.24

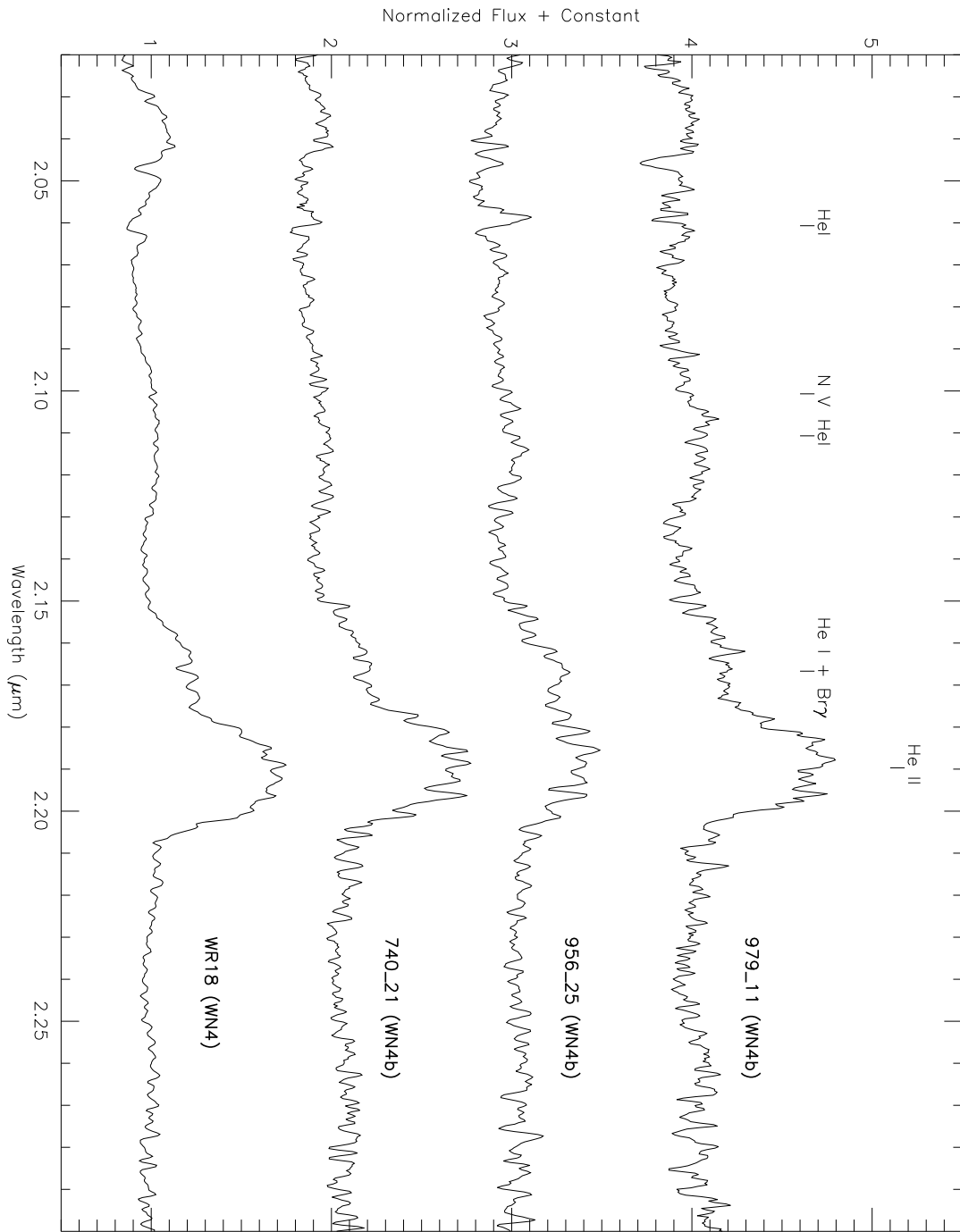


Fig. 1a.— WN4 spectra.

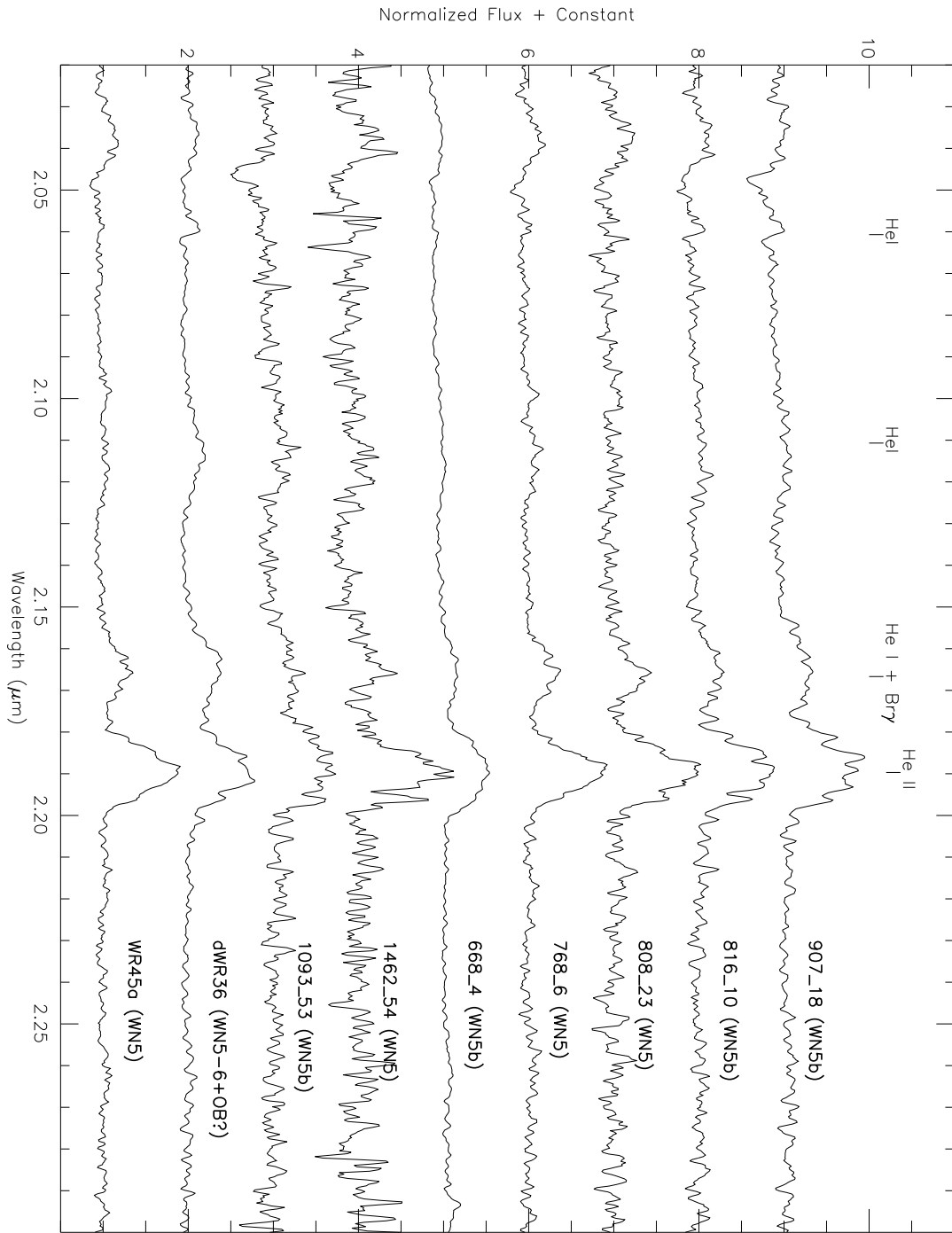


Fig. 1b.— WN5 spectra.

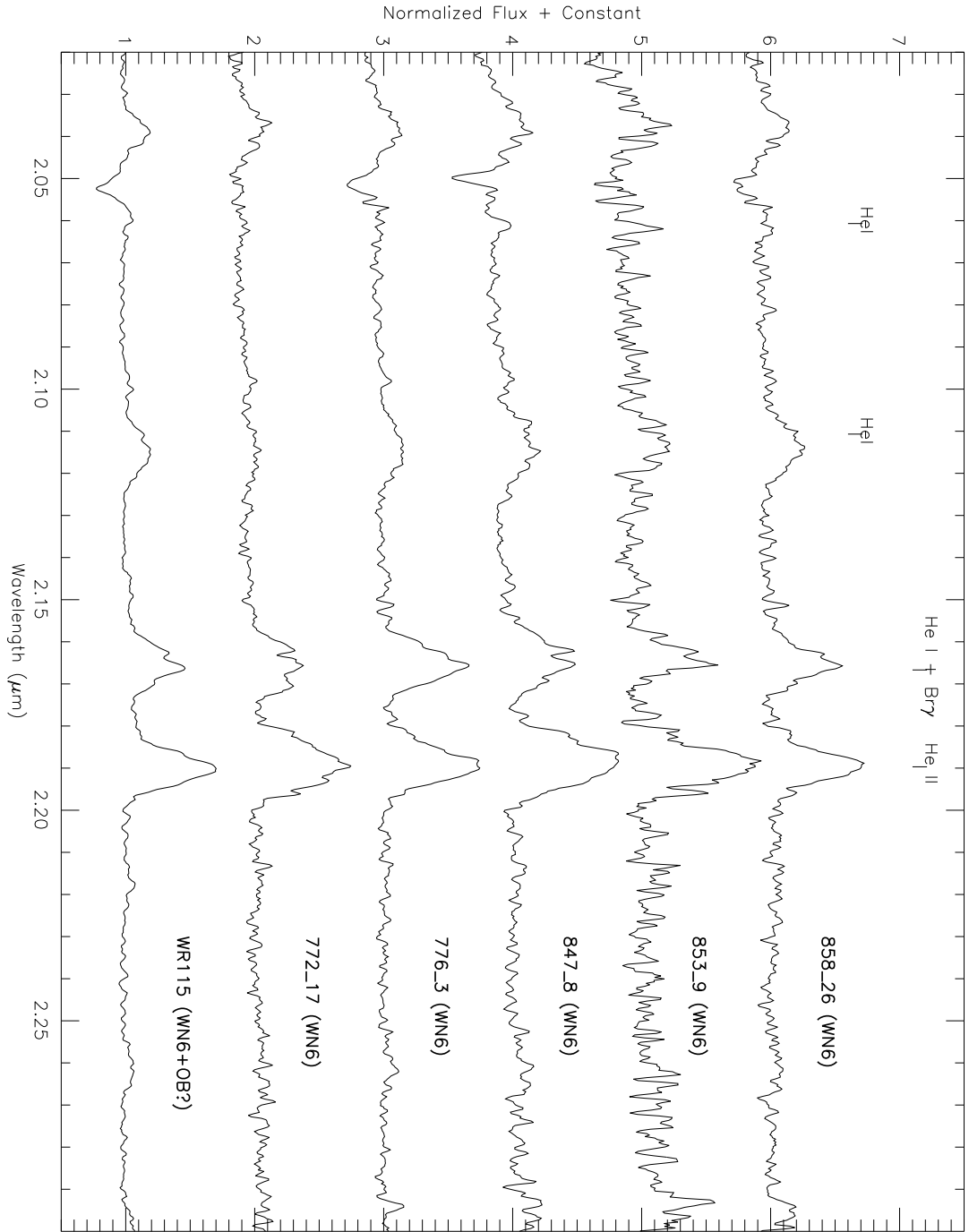


Fig. 1c.— WN6 spectra.

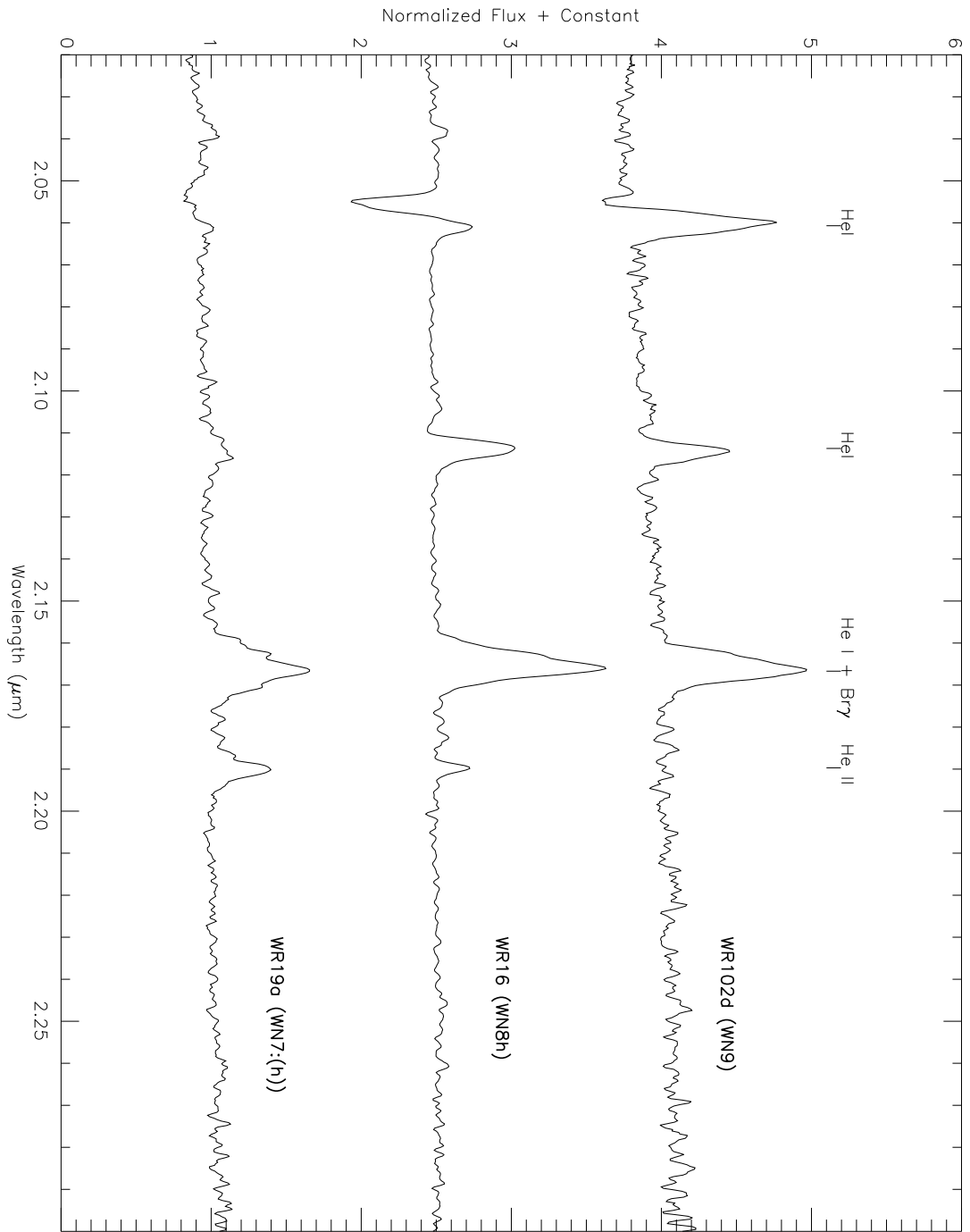


Fig. 1d.— WN7-9 spectra.

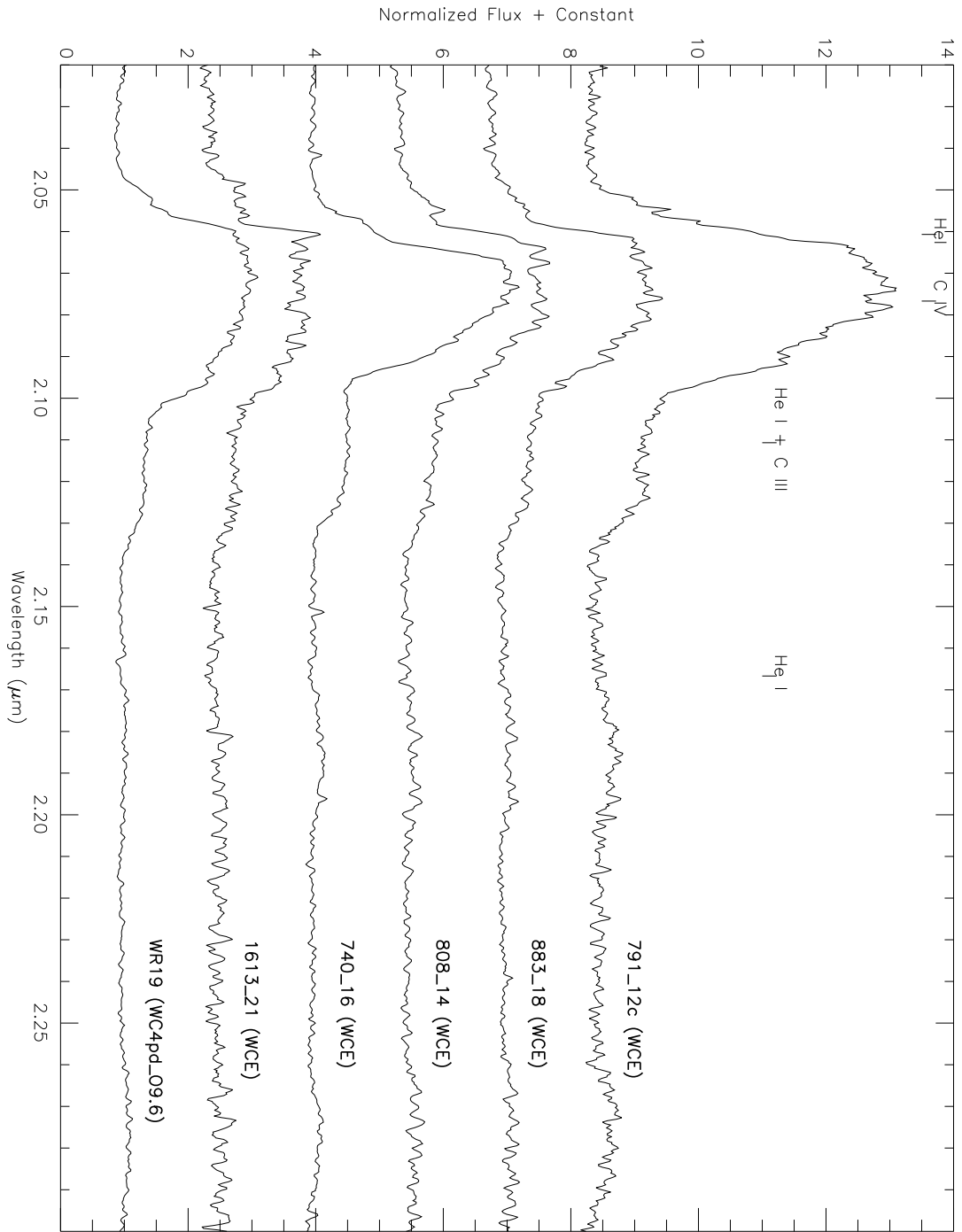


Fig. 1e.— WCE spectra.

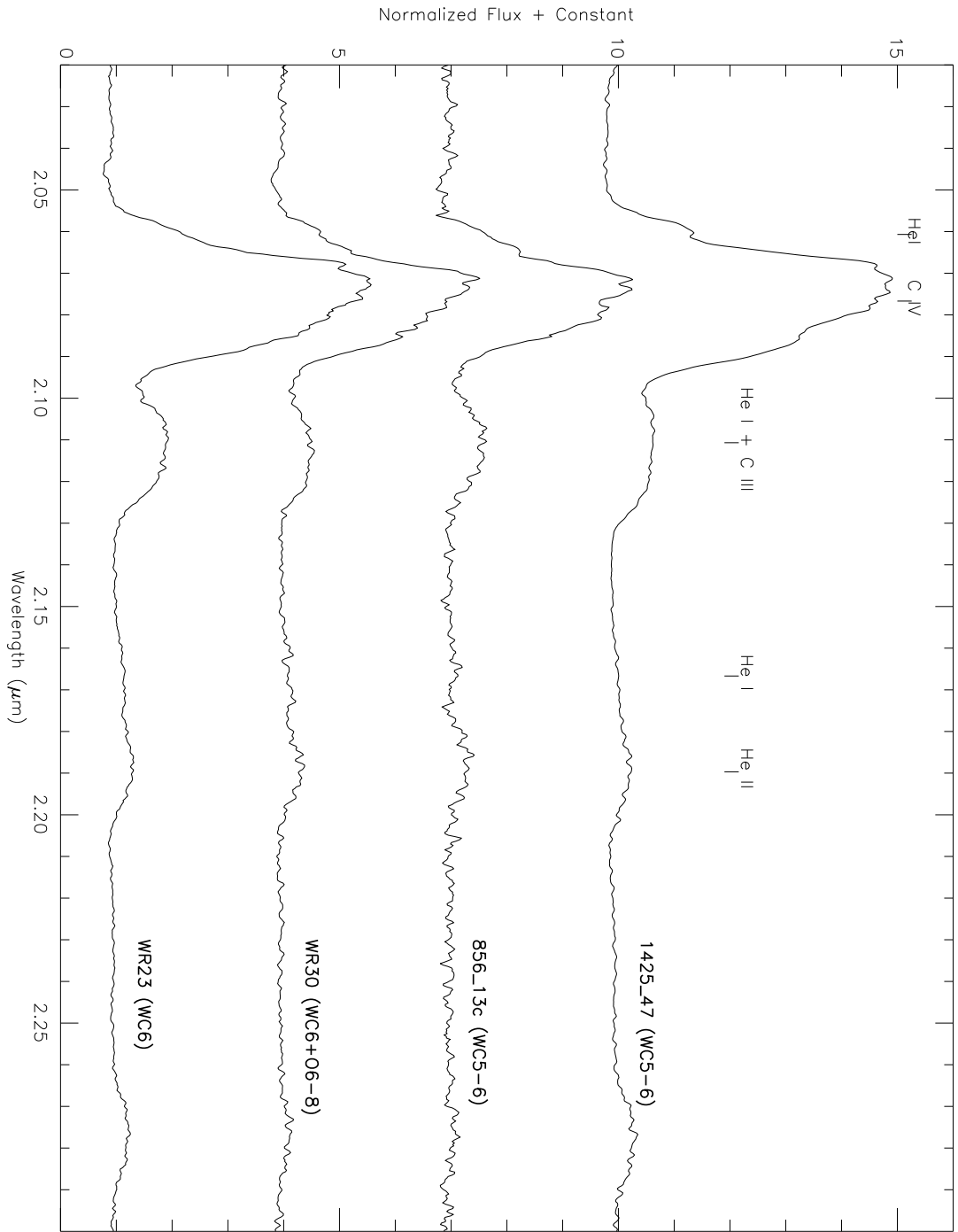


Fig. 1f.— WC5-6 spectra.

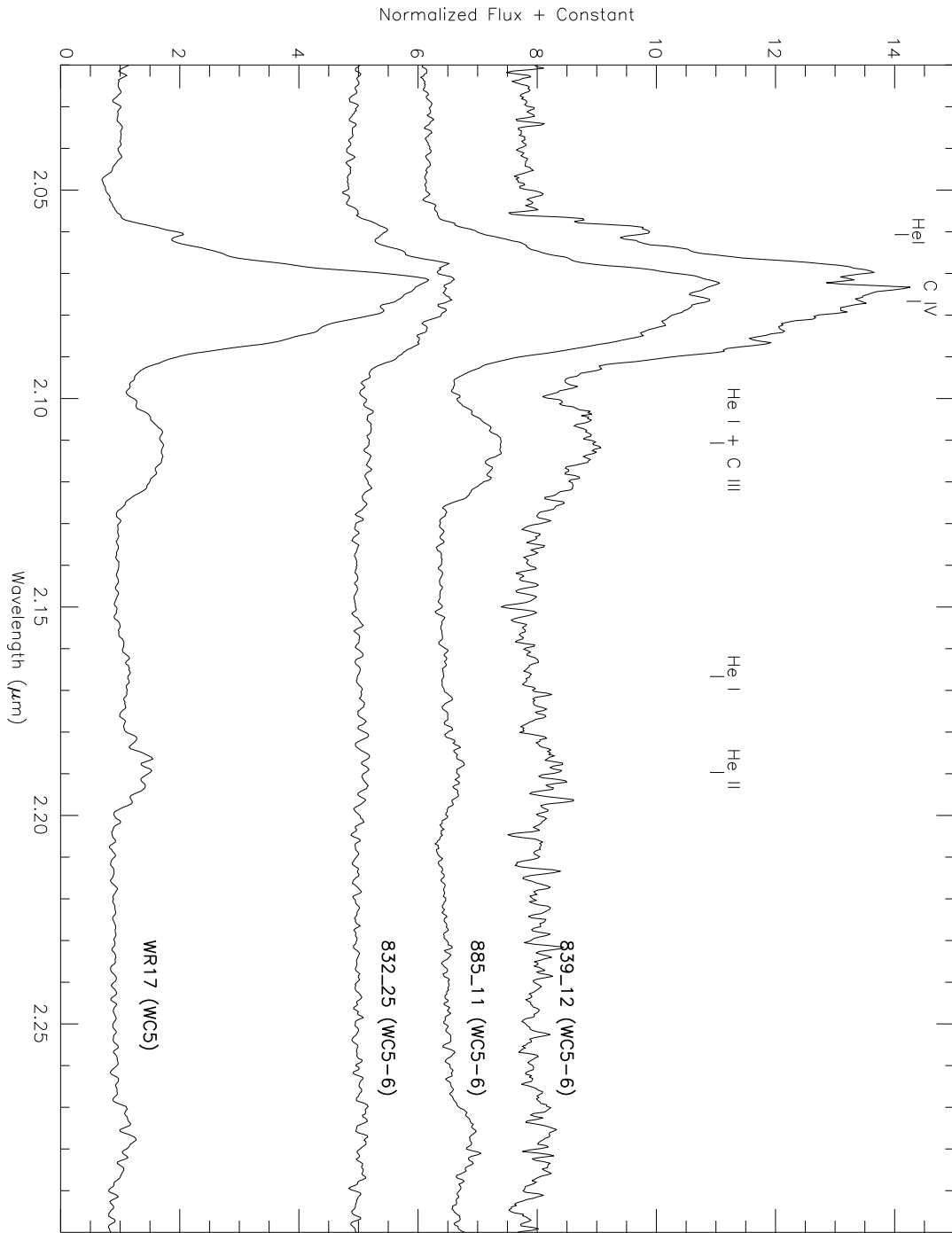


Fig. 1g.— More WC5-6 spectra.

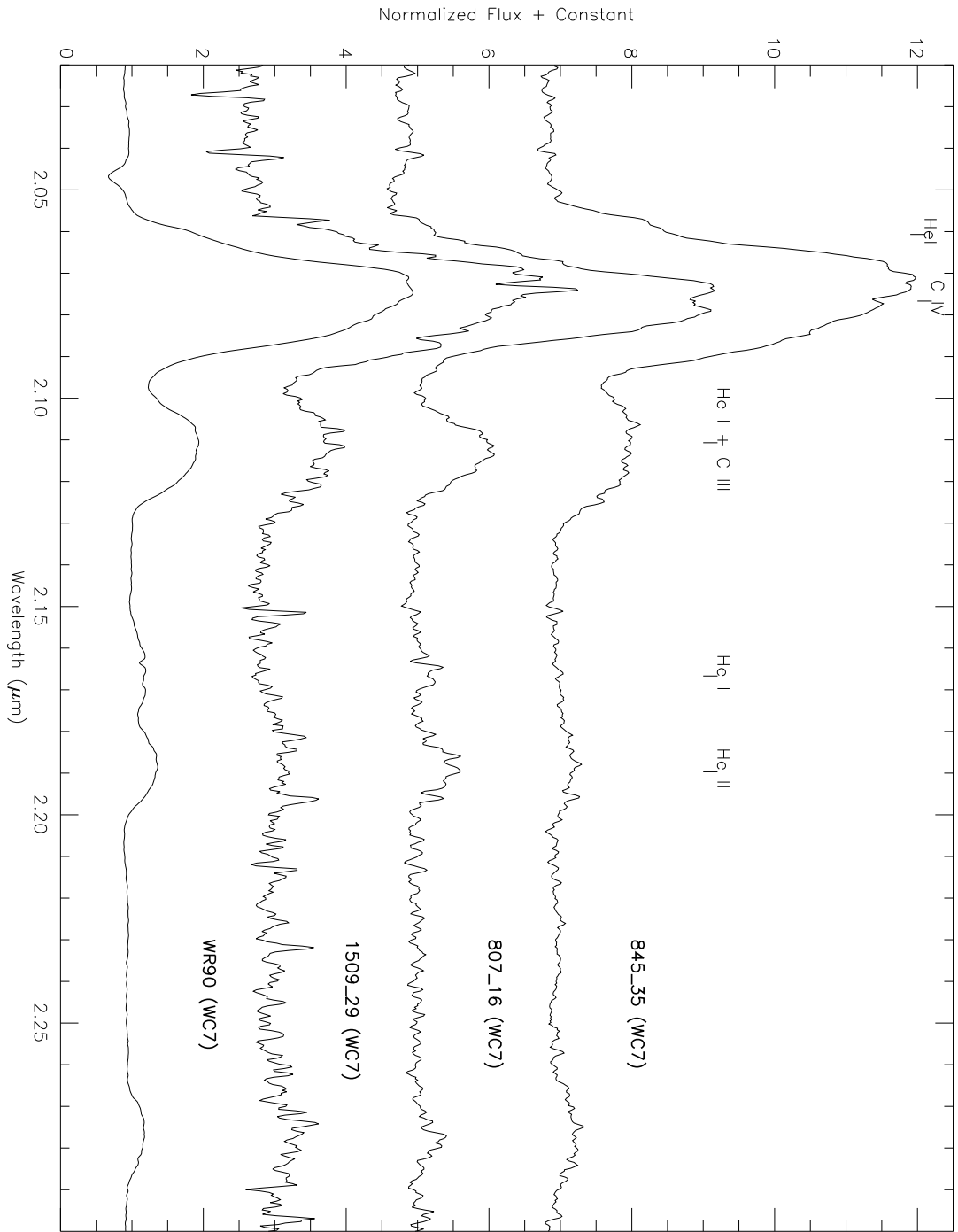


Fig. 1h.— WC7 spectra.

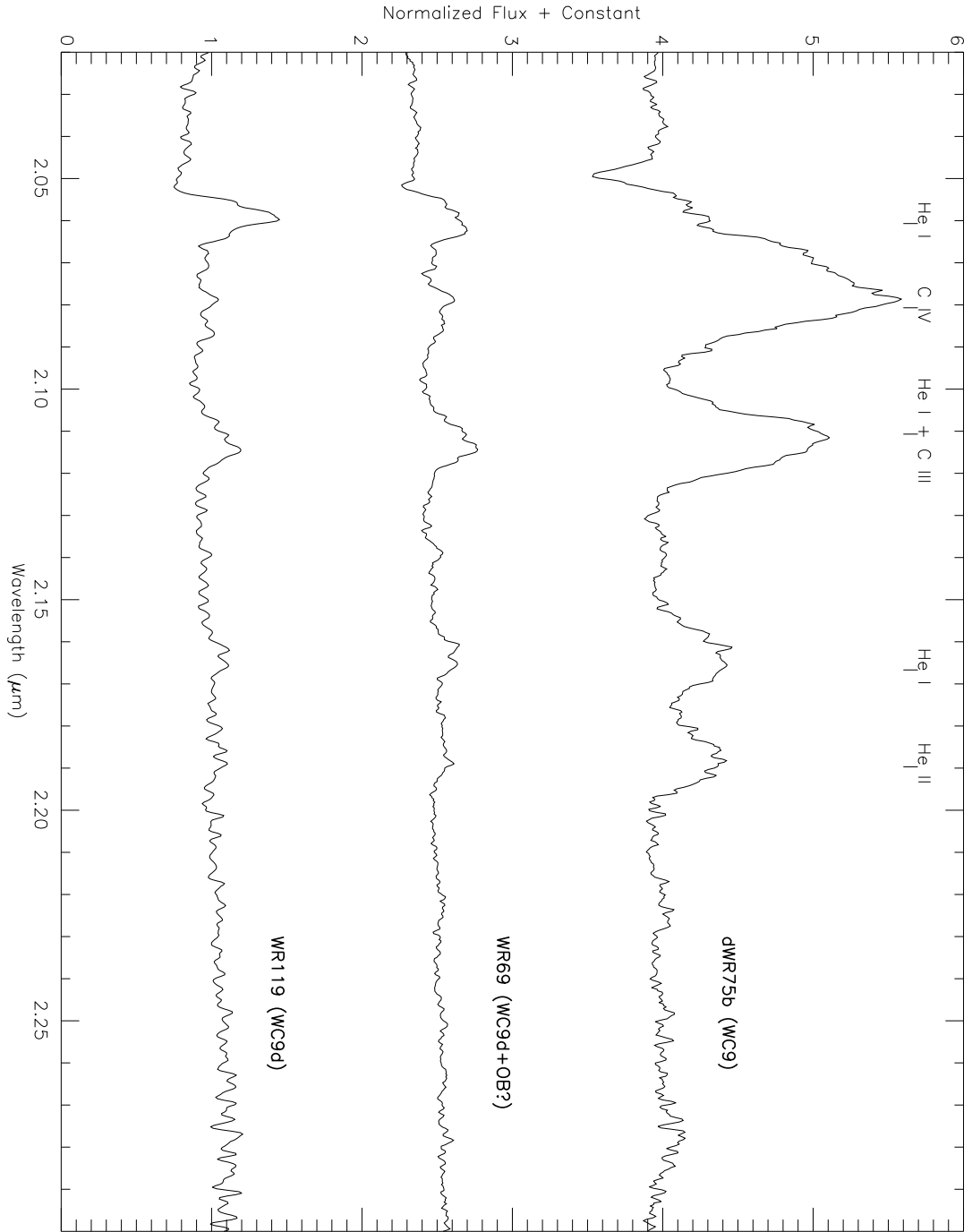


Fig. 1i.— WC9 spectra.

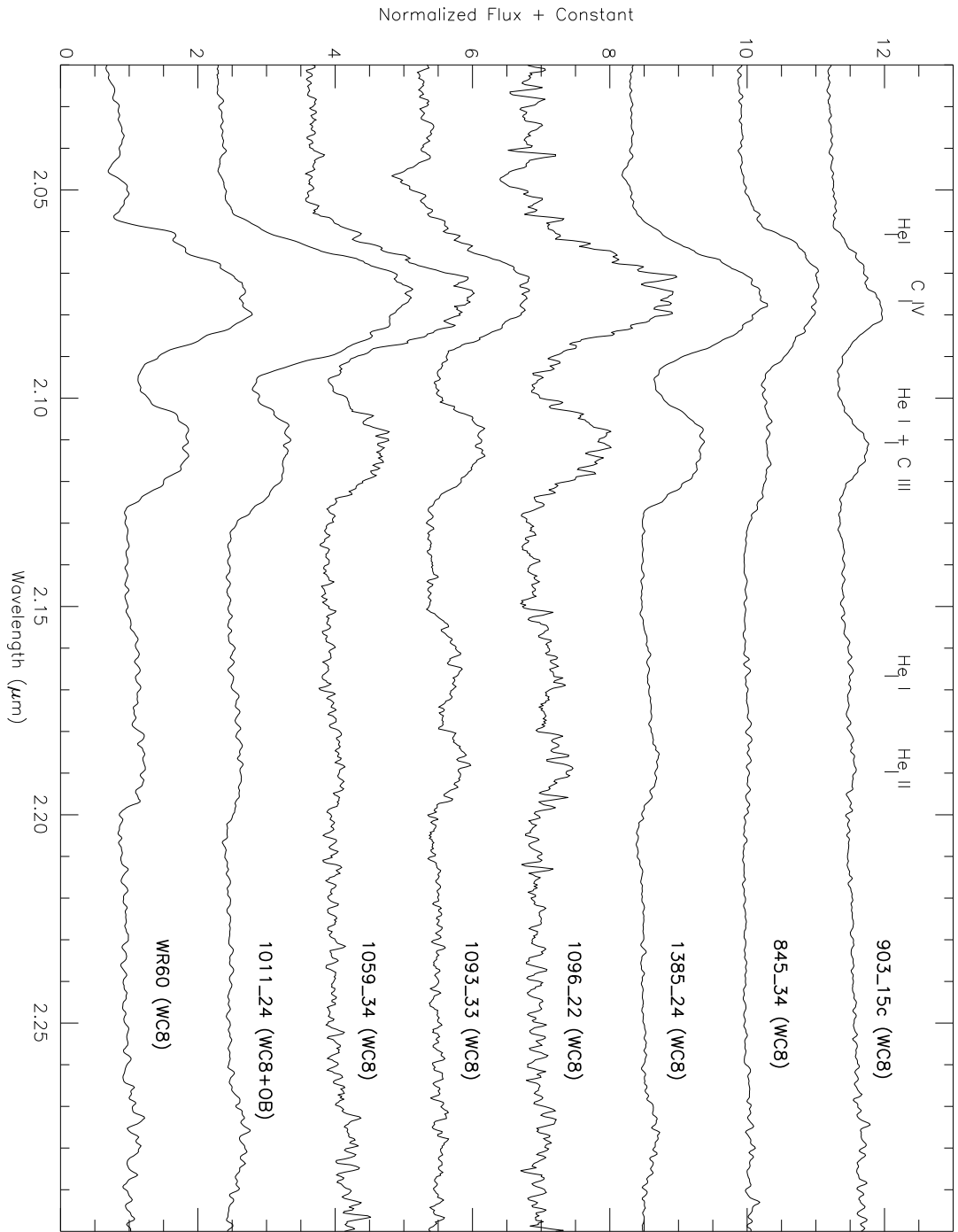


Fig. 1j.— WC8 spectra.

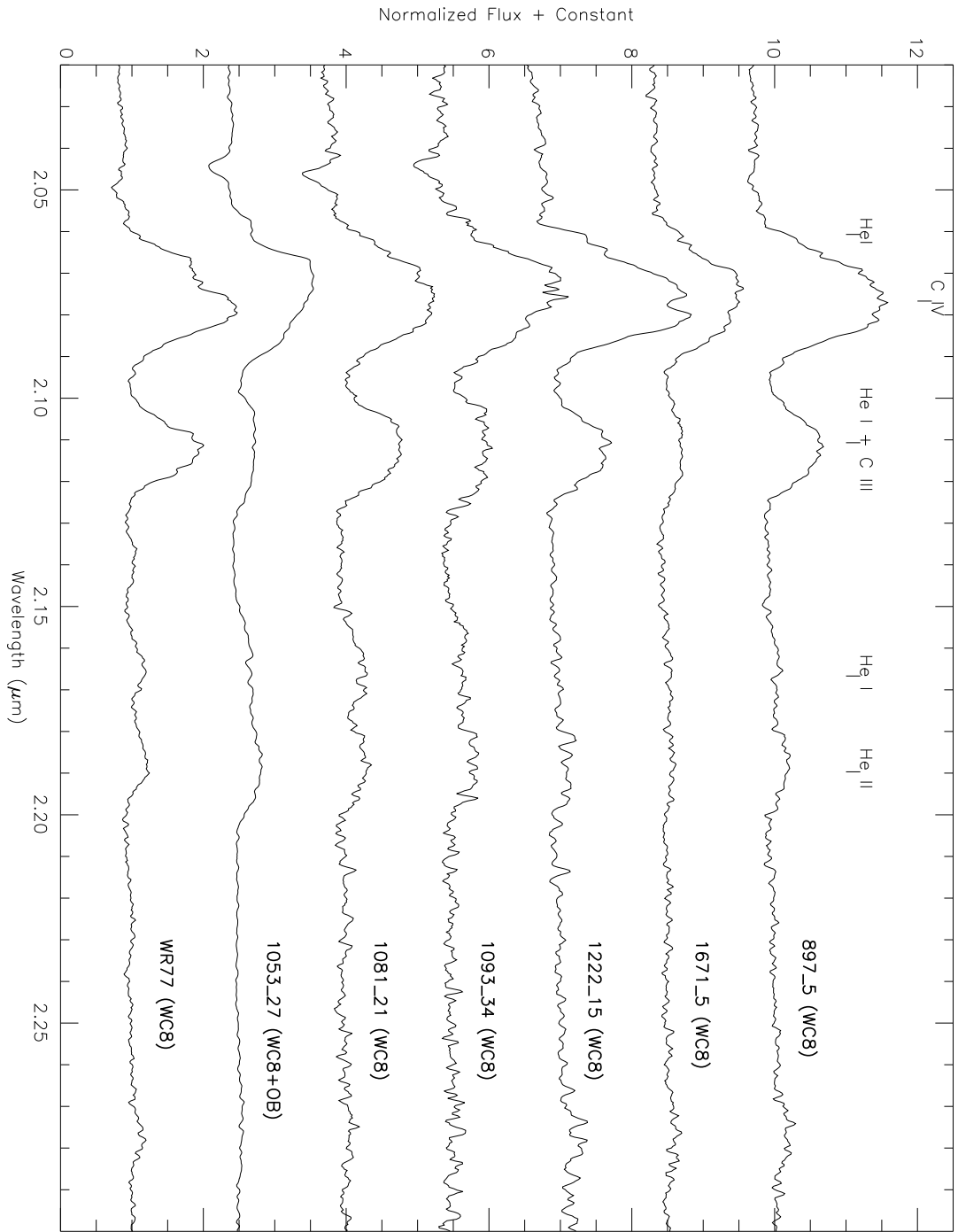


Fig. 1k.— More WC8 spectra.

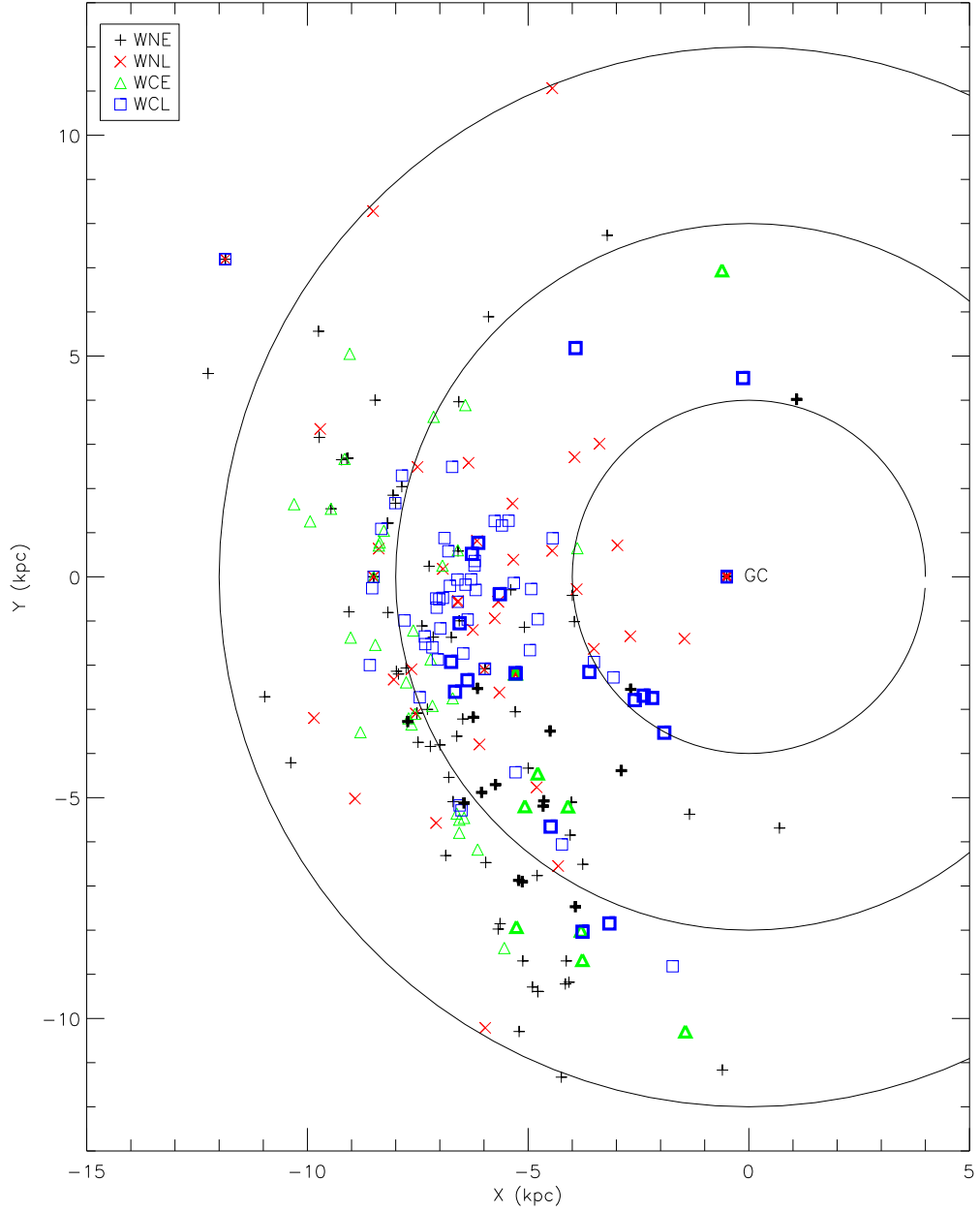


Fig. 2.— Galactic distribution of known WR stars with estimated distances, projected on the plane. New stars are represented by bold symbols.

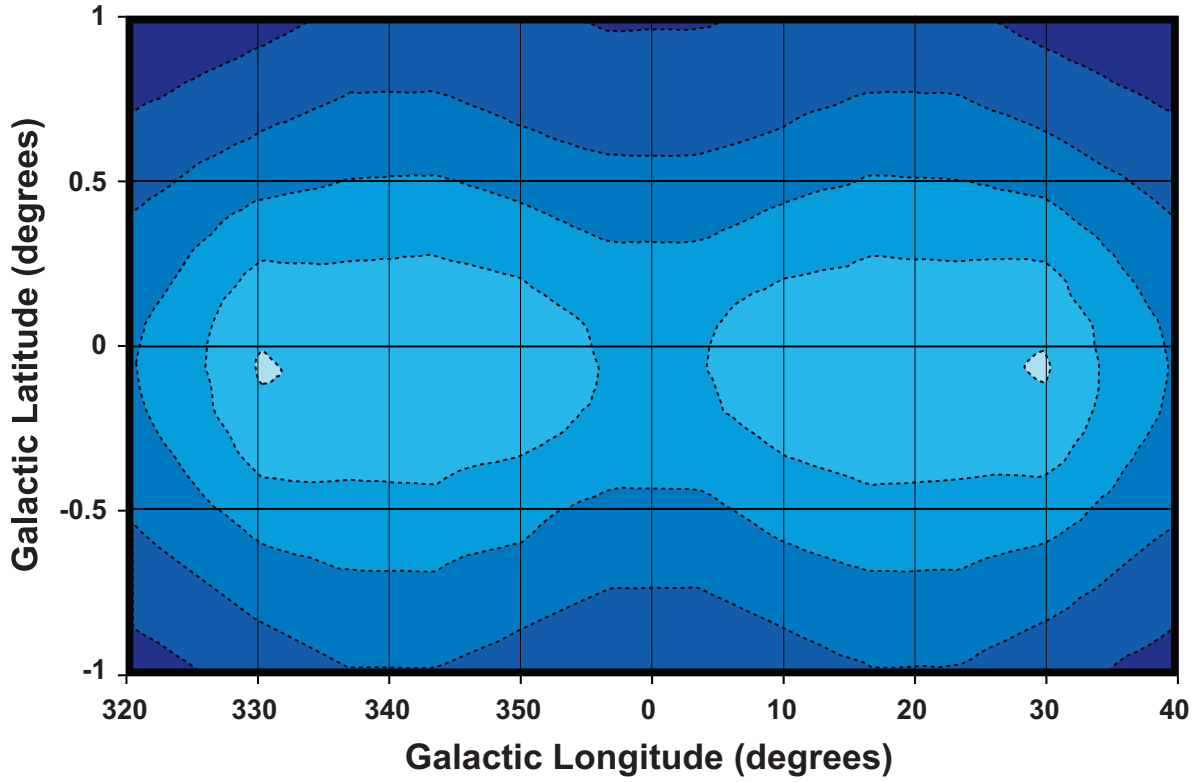


Fig. 3.— Contour plot of the target K magnitude in order to detect 95% of all WR stars along a line-of-sight. The inner contour represents a magnitude higher than 17 and each contour represents intervals of 1 mag.

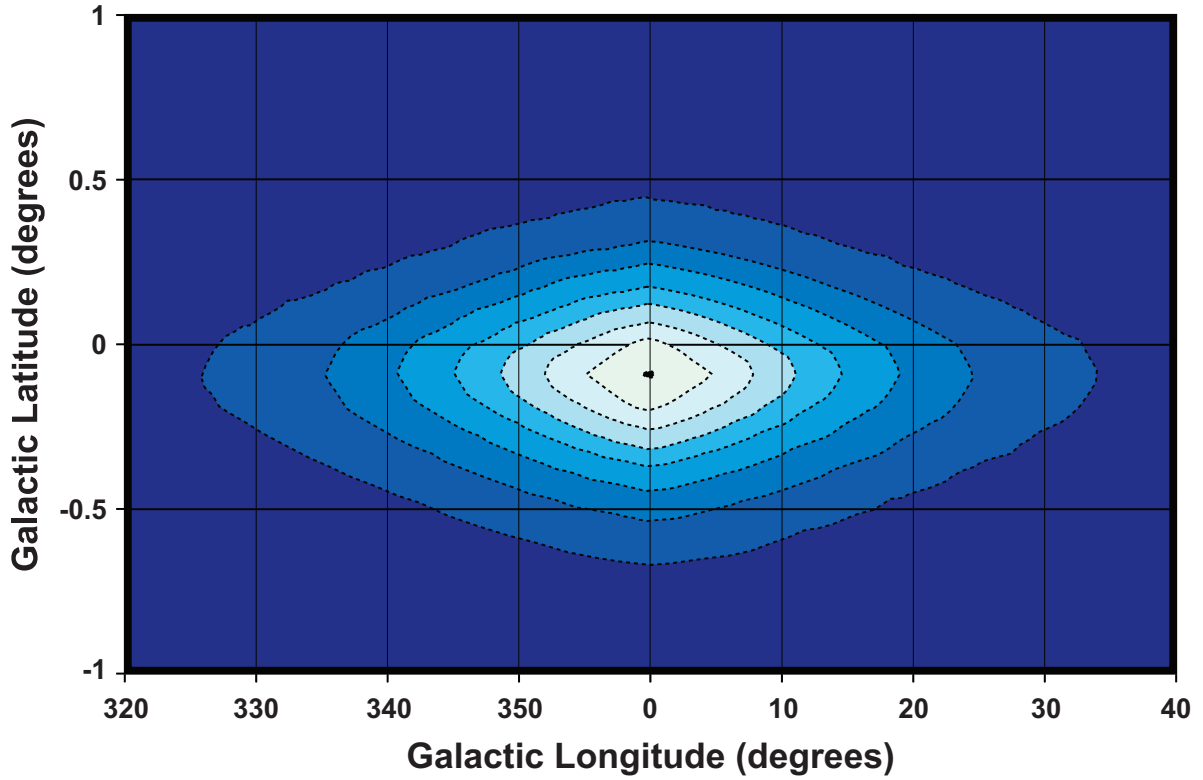


Fig. 4.— Number of WR stars along a line-of-sight within a Cpaper field ($35' \times 35'$). The inner contour represents 40 WR stars per field and each contour represents intervals of 5 WR stars per field. According to this model, ~ 5600 of all WR stars (i.e. 88%) should be found within the region: $l = 320$ to 400 and $b = -1$ to 1 .

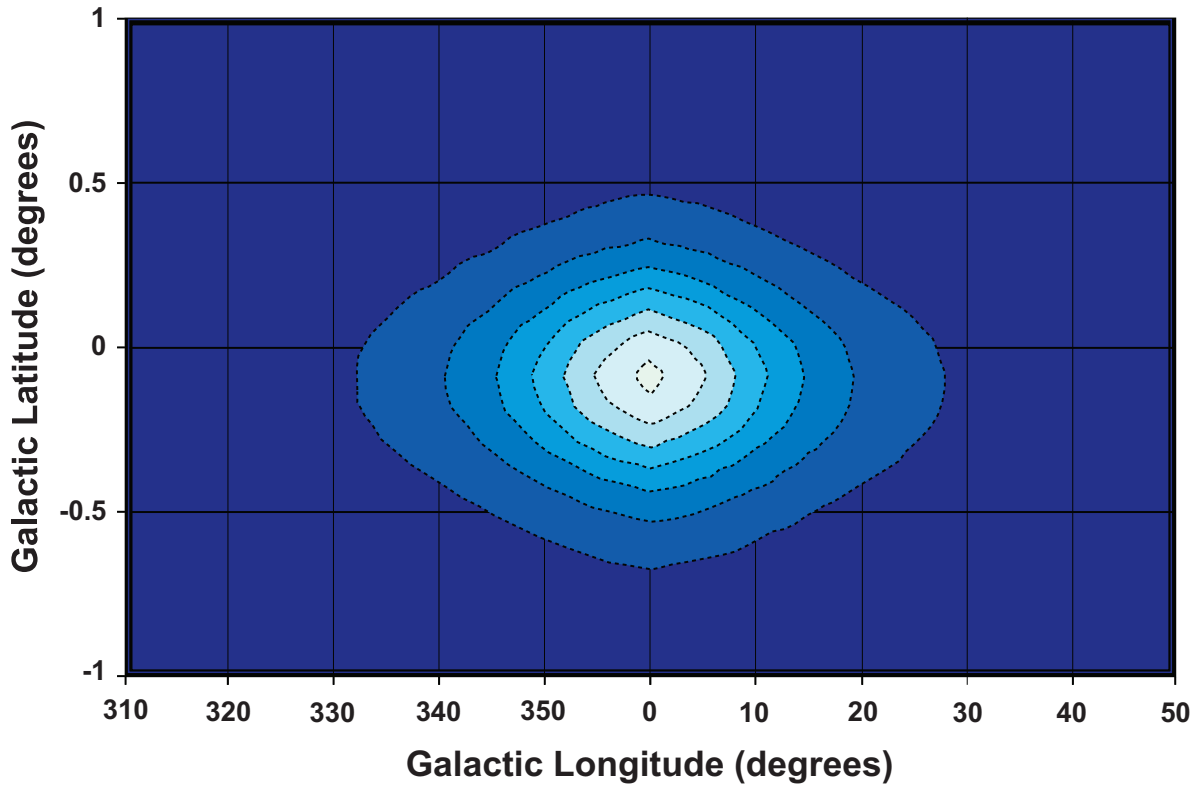


Fig. 5.— Number of WR stars along a line-of-sight within a Cpaper field up to a magnitude $K=15$. The inner contour represents 35 WR stars per field and each contour represents intervals of 5 WR stars per field.

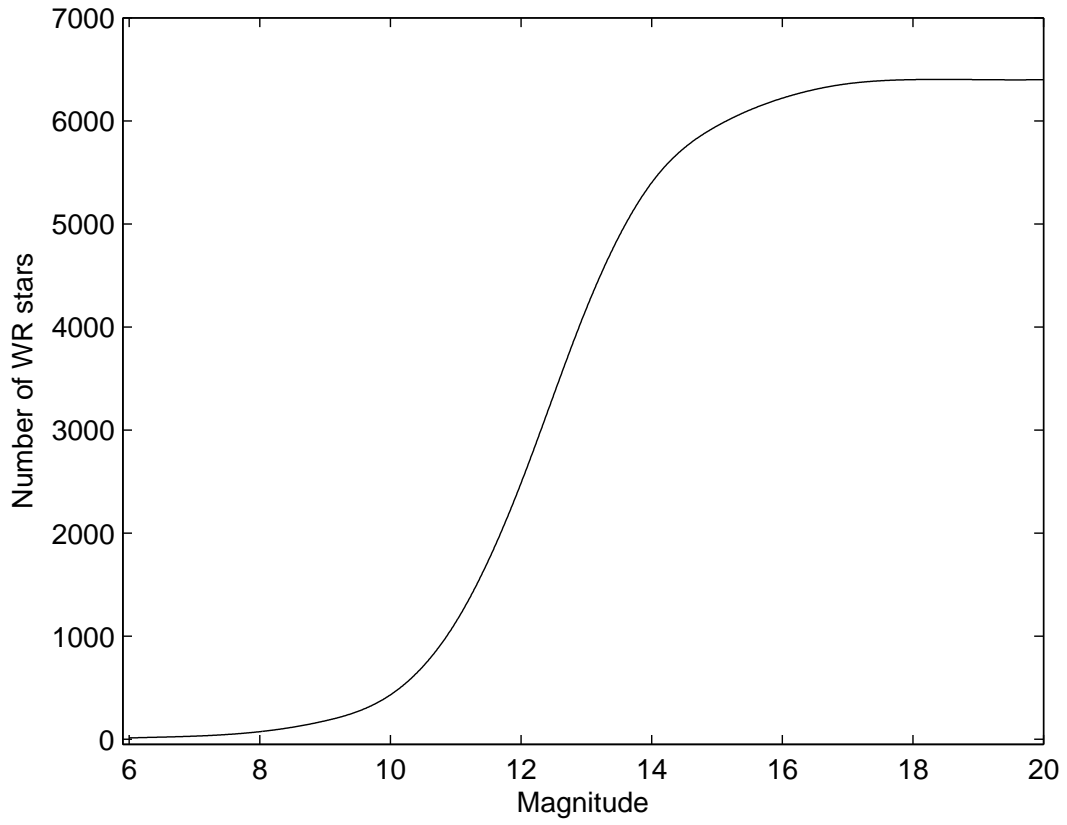


Fig. 6.— Predicted cumulative number of WR stars as a function of K magnitude.

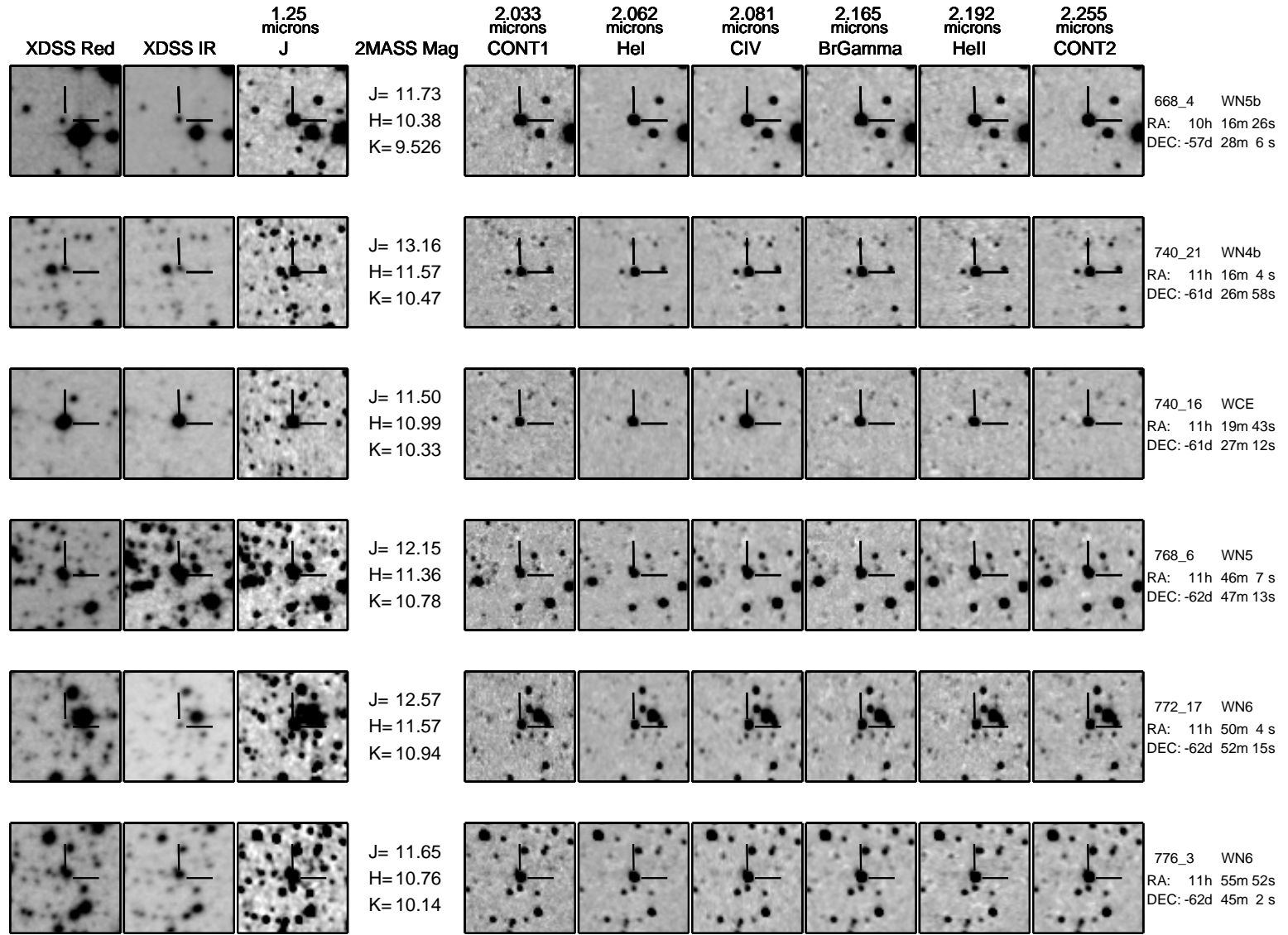


Fig. 7a.— Finder Charts for WR stars in table 2.

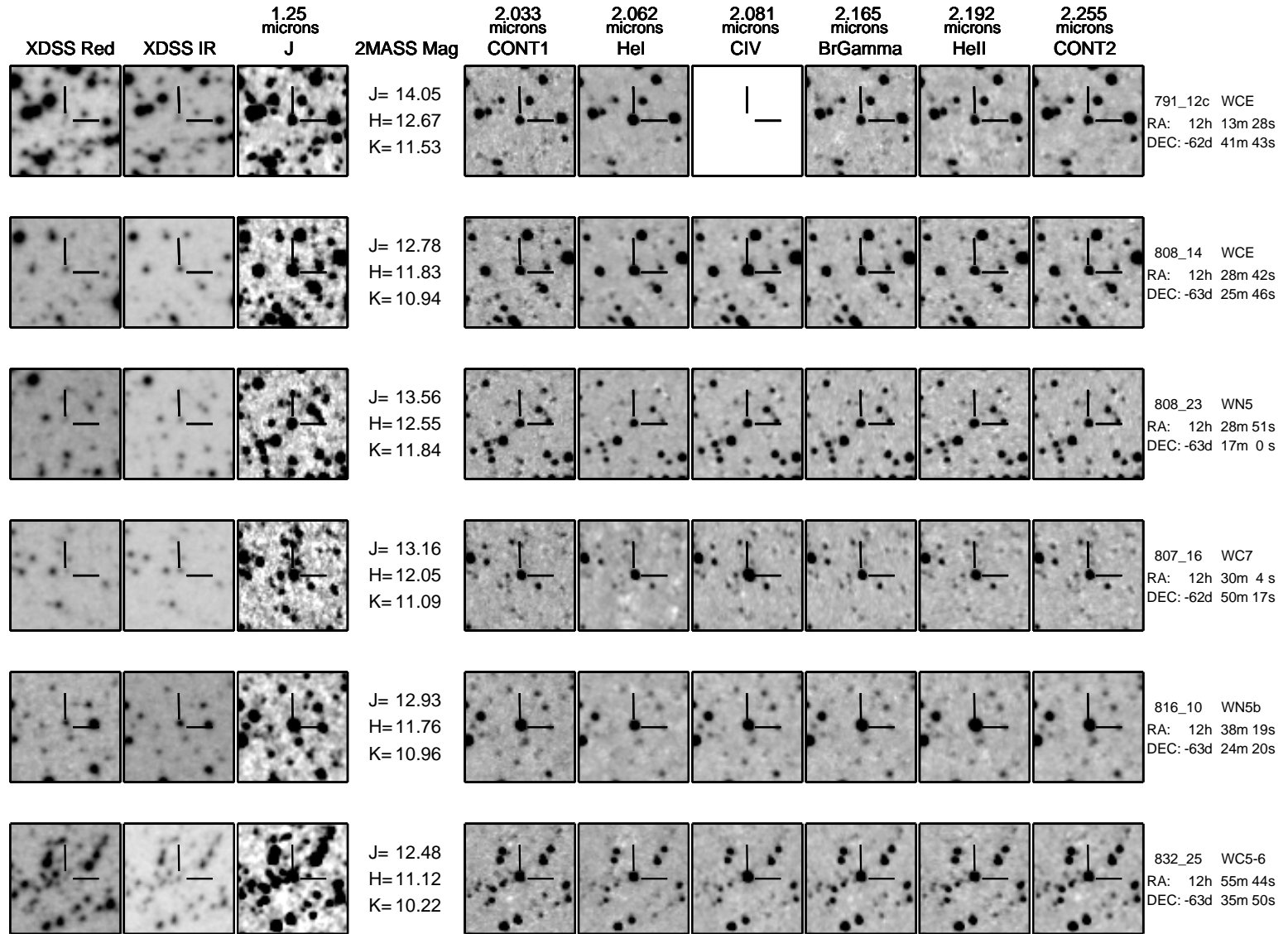


Fig. 7b. — Continued

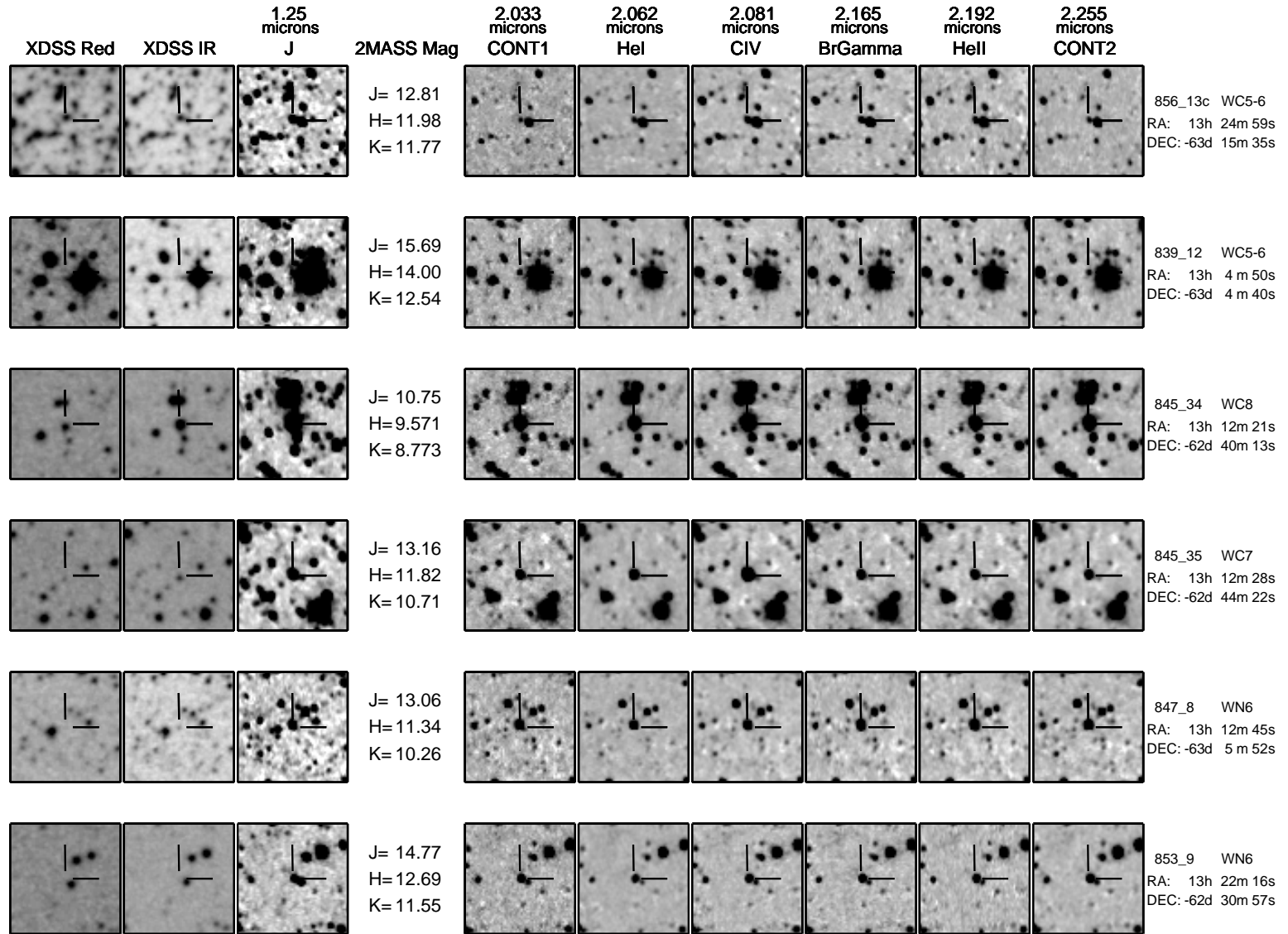


Fig. 7c.— Continued

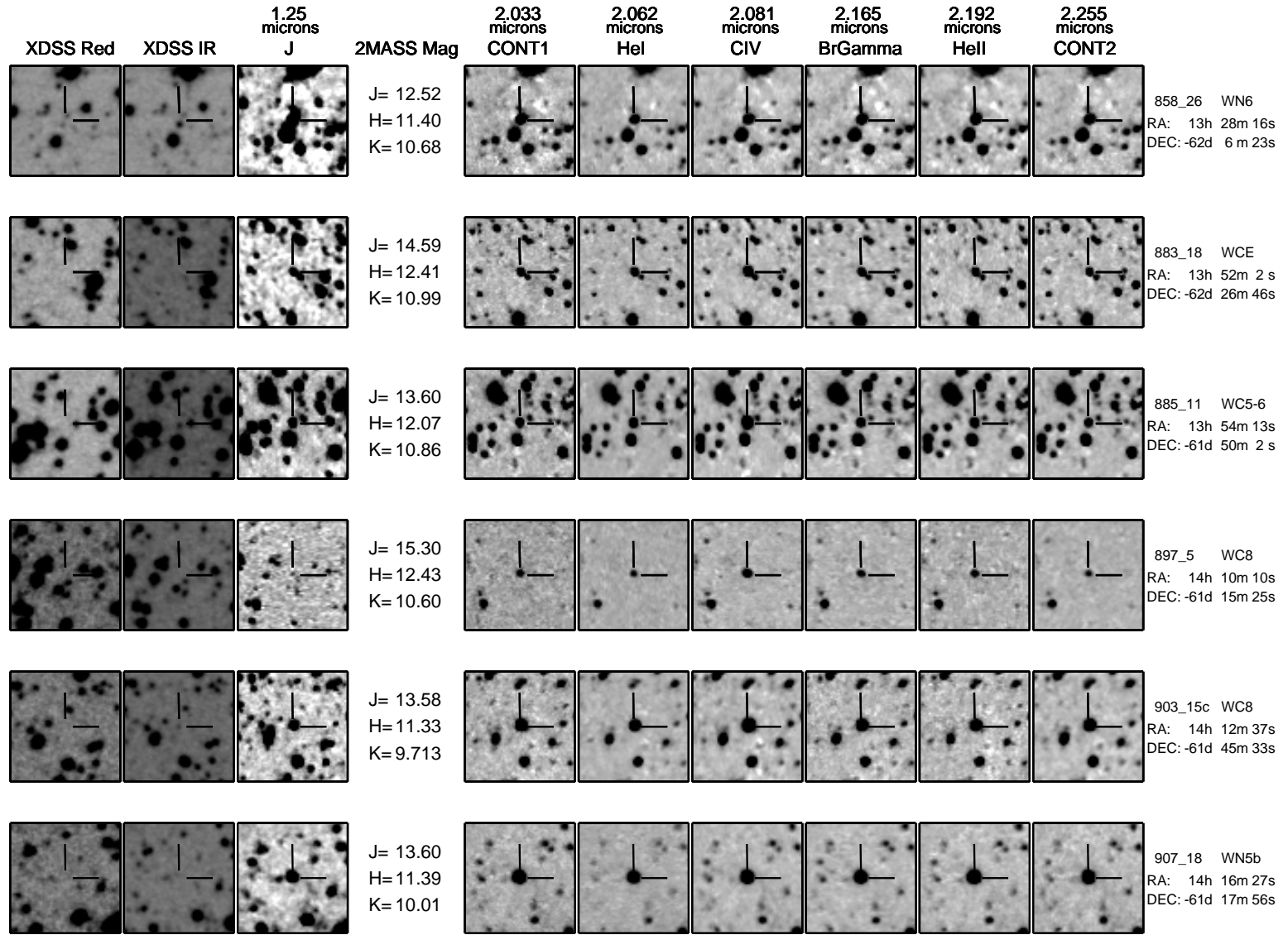


Fig. 7d. — Continued

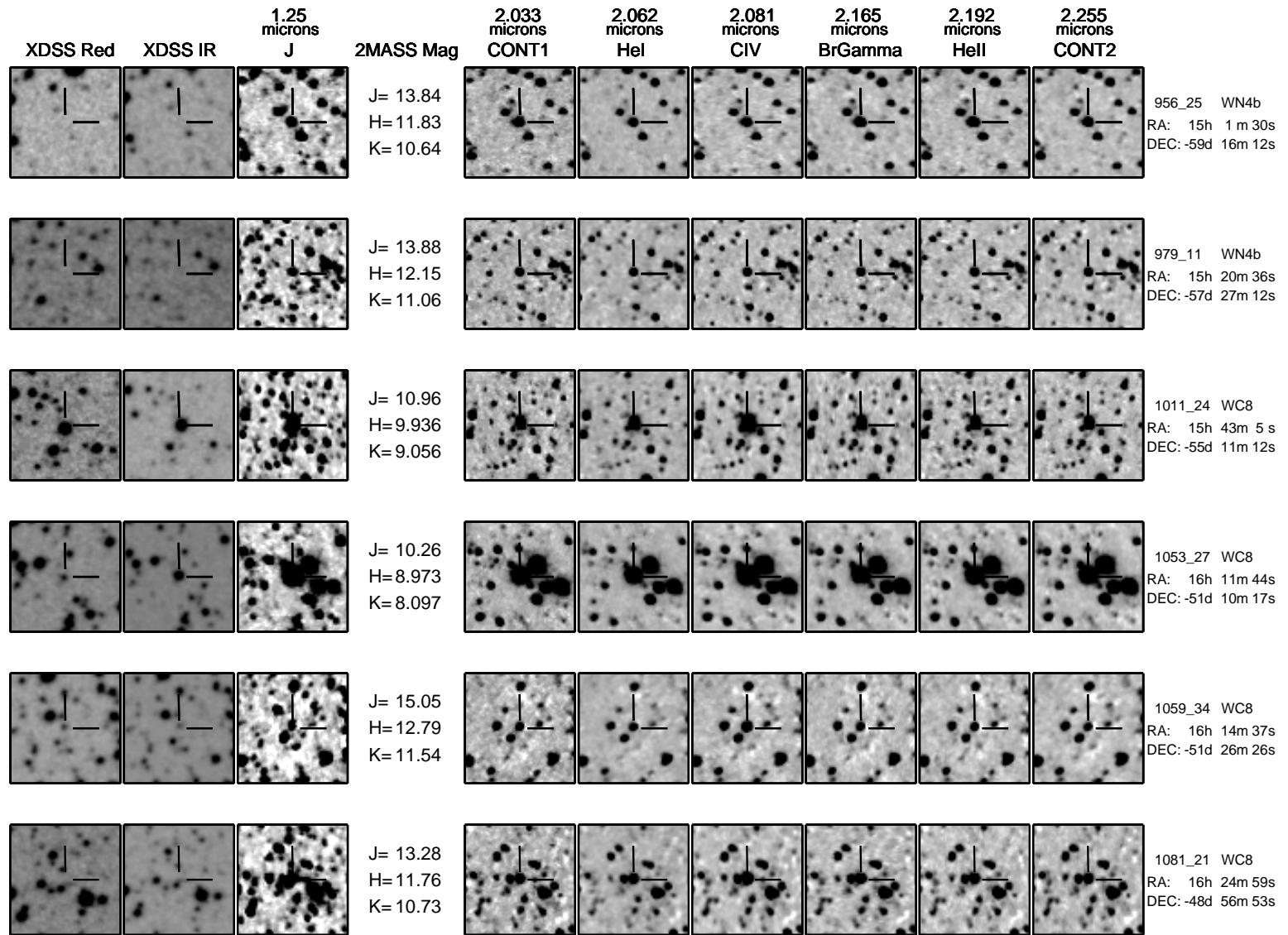


Fig. 7e.— Continued

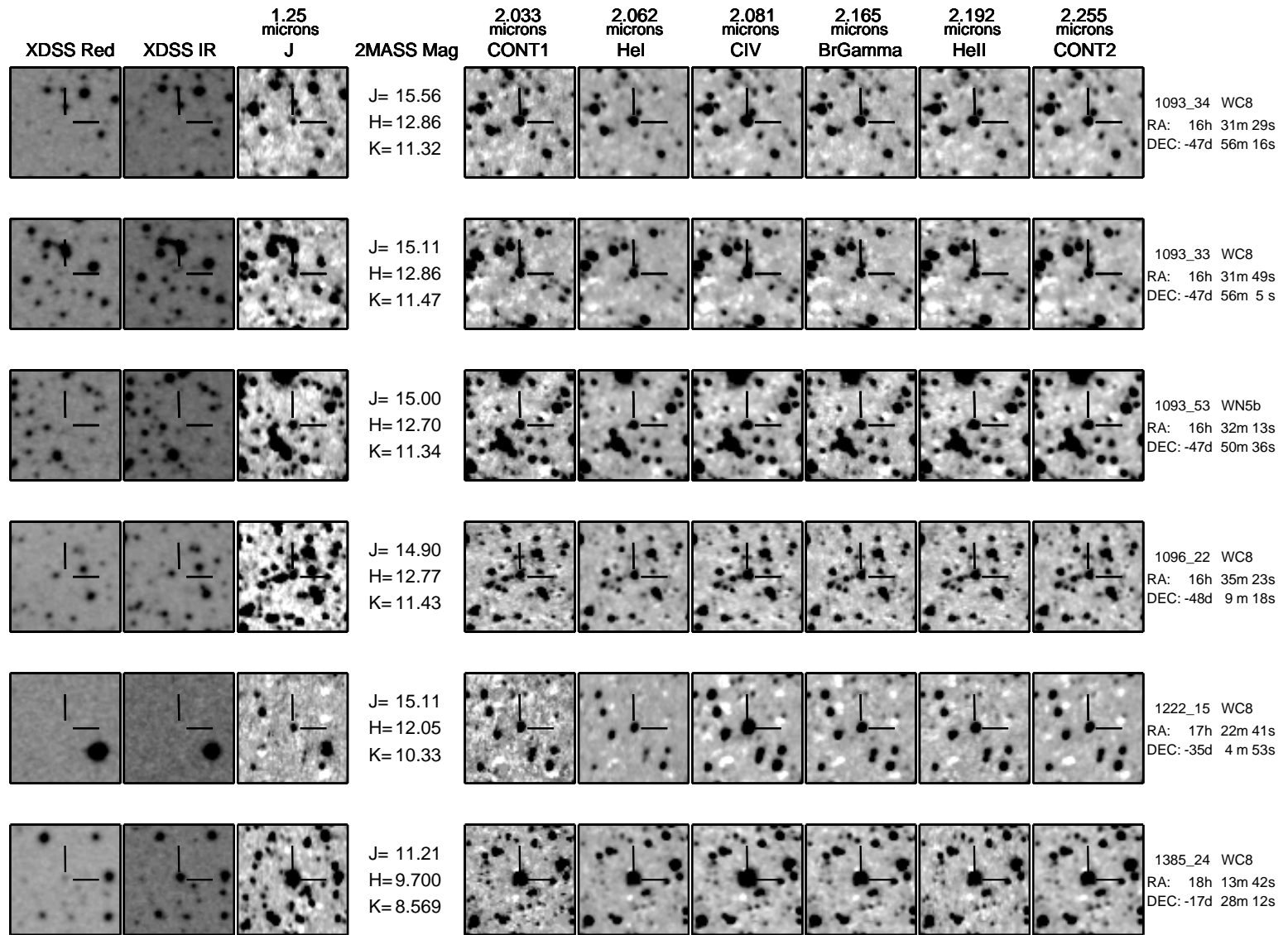


Fig. 7f. — Continued

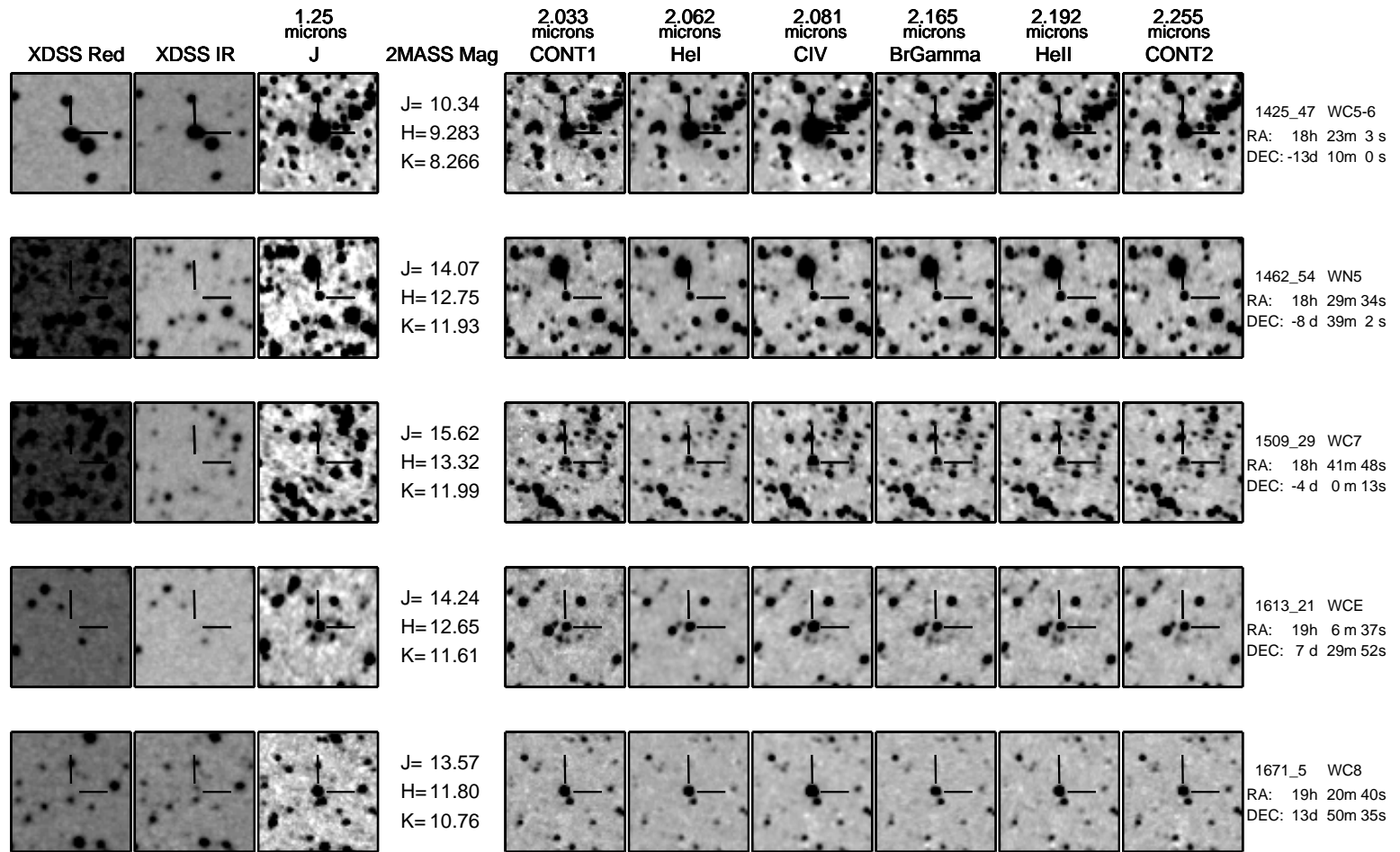


Fig. 7g.— Continued